University of Cape Town

Department of Human Biology

Division of Biomedical Engineering

in association with

Cardiovascular Research Unit

Chris Barnard Division of Cardiothoracic Surgery

Electrospun Tissue Engineered Vascular Grafts

In fulfilment of the requirements for the degree: MSc (Med) Biomedical Engineering

February 2019

Vincent Martin Hülk

Supervisor: Assoc. Prof Deon Bezuidenhout

University of Cape Town

The copyright of this thesis vests in the author. No quotation from it or information derived from it is to be published without full acknowledgement of the source. The thesis is to be used for private study or non-commercial research purposes only.

Published by the University of Cape Town (UCT) in terms of the non-exclusive license granted to UCT by the author.

University of Cape Town

DECLARATION

I, Vincent Martin Hülk, hereby declare that the work on which this dissertation/thesis is based is my original work (except where acknowledgements indicate otherwise) and that neither the whole work nor any part of it has been, is being, or is to be submitted for another degree in this or any other university.

I empower the university to reproduce for the purpose of research either the whole or any portion of the contents in any manner whatsoever.

Signature: Signed by candidate

Date: 11/02/2019

Abstract

ePTFE and Dacron vascular grafts are successful in large diameter applications but provide poor outcomes in small diameter (<6 mm) applications. Occlusion, poor cell ingrowth and a mismatch of compliance compared to the native vessel, cause failure to the current synthetic grafts. Spontaneous transmural endothelialisation can be enhanced in non-degradable scaffolds with heparin-mediated growth factor delivery via heparin surface modification, as well as induce an anti-thrombotic lumen. Electrospinning of vascular grafts offer a means to mimic the natural extracellular matrix (ECM) with improved porosity and pore for increased cell ingrowth, incorporation of drugs for sustained release, and tailoring mechanical properties match that of the native vessel. This study aims to produce a small diameter biodegradable vascular graft with sufficient porosity/pore size and incorporated heparin as an angiogenic/anti-thrombotic agent.

DegraPol® (DP30), a degradable polyurethane was dissolved in different ratios of chloroform/HFIP (24%w/w) and electrospun at 30%, 40%, and 50% rH to obtain a small diameter vascular graft with improved porosity/pore size and mechanical properties. The sodium salt of heparin ($HepNa^+$) was modified to heparin tributylamine (HepTBA) to ensure the solubility in organic solvents and incorporated into the electrospinning solution at 3% and 5% wt/wt (w HepTBA/w polymer). The grafts were analysed for morphological (fibre diameter, porosity/pore size, fibre alignment) and mechanical (hoop stress, strain, burst pressure, compliance) properties. After *in vitro* elution and degradation studies, grafts (DP30 and DP30+3%HepTBA) were evaluated in an *in vivo* pilot study using a rat infrarenal aortic interposition model (28 days).

Relative humidity did not significantly influence the scaffold morphology or the mechanical properties, for solvent systems used. However, the addition of HFIP to the solution had on average a 2.9-fold decrease in the circumferential UTS and strain from 0.63±0.16 MPa and 90±16%, respectively. The grafts showed theoretical compliance in the physiological range of 6-8%/100mmHg and showed a significant amount of drug release in the first 5 days and a cumulative release of 62% and 36% (respectively) by day 28. The DP30 and DP30+3%HepTBA grafts lost 46% ($P>0.5$) and 50% ($P<0.01$) of its circumferential UTS respectively, whereas the loss in maximum strain for the same groups was 66% ($P<0.0001$) and 76% ($P<0.01$). A porosity of 64.5±2.7% and 54.9±2.2% ($P<0.01$) was achieved for the DP30 and DP30+3%HepTBA with 52% and 29% of the pore sizes larger than 10 µm. The *in vivo* pilot study showed patent grafts with tissue ingrowth and endothelium on the lumen for DP30 as well as the DP30+3%HepTBA group.

The DP30 grafts show promise for the replacement of small diameter vessels. Heparin-eluting grafts will be further evaluated in long-term isolated loop models to determine their capacity for spontaneous transmural endothelialisation.

Graphical Abstract

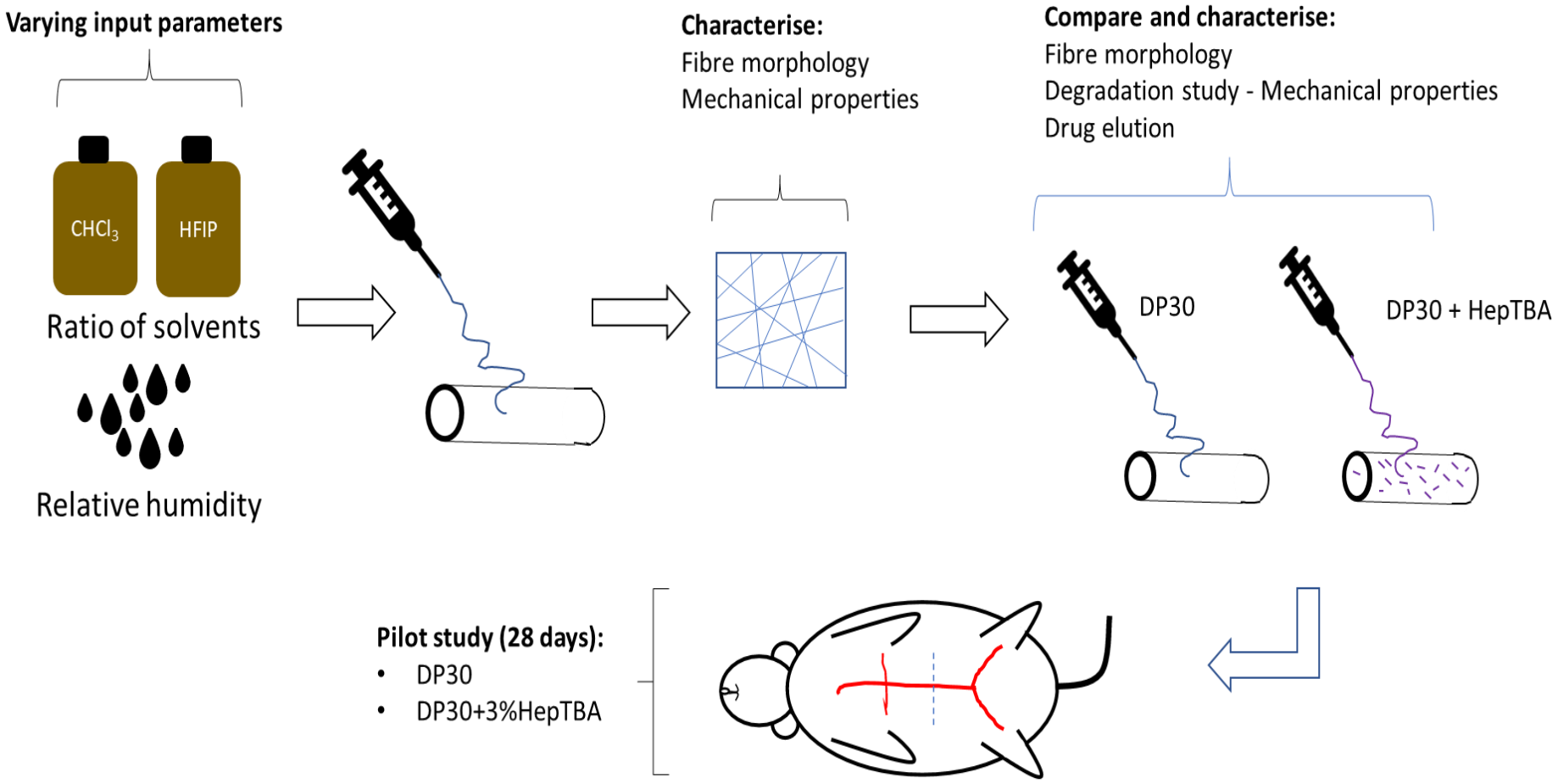

Acknowledgements

Firstly, I would like to thank Assoc. Prof Deon Bezuidenhout for his guidance and mentorship through these two years. His work ethic and enthusiasm are traits that I will always draw inspiration from and will take this with me into the future.

A special thanks to dearest mother, Erika, and father, Martin, for the sacrifices they have made for me to be here. I can never be grateful enough for their support and encouragement through every moment of my life. Thanks to my lovely sister, Siobhan, for her positive attitude towards life and for my grandparents for their moral support while studying in Cape Town.

I would like to thank the following incredible people – Anel Oosthuysen (lab assistance), Joel du Toit (technical support), Damita Zireva (electrospinning), Wesley Elson and Johan Coetzee (electronic support and design), Janet McCallum (animal welfare), Helen Ilsey (histology) and Andrew Lin, Rosslee Guess, Olivia Wimberley, and Sibusisiwe Maseko for keeping up the moral in the laboratory. A special thanks to Wian van den Bergh for his patience and being my electrospinning expert, Natercia da Silva for doing the implants for the pilot study in her personal free time.

I would like to acknowledge the National Research Foundation (NRF) of South Africa, the Cardiovascular Research Unit, and the University of Cape Town for making the funds available for this project.

Lastly, I want to praise the Saviour for bestowing His grace upon my life, for that I will forever be thankful and humbled.

Contents

List of Figures

List of Tables

List of Abbreviations

bFGF	Basic fibroblast growth factor
C	Circumferential
$CHCl_3$	Chloroform
DI	Deionised water
DMF	Dimethylformamide
DP30	DegraPol® 30
EC	Endothelial cell
ECM	Extracellular matrix
ePTFE	Expanded polytetrafluoroethylene
EtOH	Ethanol
FGF	Fibroblast growth factor
Gags	Glucosaminoglycans
GF	Growth factor
H&E	Hematoxylin and Eosin
HCl	Hydrochloric acid
$HepH^+$	Heparin acid
$HepNa^+$	Heparin sodium
HepTBA	Heparin-tributylamine
HFIP	Hexafluoroisopropanol
ID	Internal diameter
KCl	Potassium chloride
L	Longitudinal
LTE	Low temperature electrospinning
MBTH	Methyl benzothiazolinehydrazone hydrochloride
MC	Dichloromethane
MeOH	Methanol
MSCs	Mesenchymal stem cells
NaCl	Sodium chloride
NaOH	Sodium hydroxide
NMR	Nuclear magnetic resonance
OI	Orientation index
OD	Outside diameter
PBS	Phosphate buffered saline
PCL	Polycaprolactone
PDGF	Platelet-derived growth factor
PEG	Polyethylene glycol
PEO	Polyethylene oxide
PEUU	Poly(ester urethane) urea
PGA	Polyglycolic acid
PGS	Polyglycerol sebacate
PLA	Polylactic acid
PLCL	Poly(lactide-co-caprolactone)
PLGA	Poly(lactic-co-glycolic acid)
PLLA	Poly-L-lactic acid
Por	Porosity
PS	Pore size

PU	Polyurethane
rH	Relative humidity
RT	Room temperature
SAVC	South African Veterinary Council
SEM	Scanning electron microscope
SMC	Smooth muscle cell
TA	Transanastomotic
TBA	Tributylamine
TEVG	Tissue engineered vascular graft
TM	Transmural
TPU	Thermoplastic polyurethane
UTS	Ultimate tensile strength
VEGF	Vascular endothelial growth factor

List of Symbols

C_d	Diametral compliance
D	Diameter
Ey	Young's Modulus
F	Force
m	Mass
n	Sample size
P	Pressure
V	Volume
r	Radius
T	Temperature
t	Wall thickness
w	Width
°	Degree

Greek letters

ε	Strain
ρ	Density
σ	Tensile stress

1 Introduction

1.1 Background

1.1.1 The Impact of Cardiovascular Diseases

Cardiovascular diseases are among the leading causes of death in western countries and account for 28% of deaths in South Africa (1). In the United States, $25 billion are spent on 400 000 coronary artery bypass graft (CABG) procedures, which contributes to the 3 million annual CABG procedures (2). According to Stehouwer, Clement (3) atherosclerosis is responsible for almost one-half of all the deaths in Europe. Atherosclerosis causes hardening and build-up of plaques in the tunica intima, thereby reducing the cross-sectional area and decreasing blood flow (4). Peripheral artery diseases can lead to cramping and limb amputation, due to constriction of the arteries, after which femoral/popliteal bypass surgery is often required (Figure 1-1). Coronary artery disease has more severe consequences which may lead to a heart attack and death. In advanced conditions, where medical or minimally invasive procedures such as stenting are not viable options, the artery needs to be replaced or bypassed with a vascular graft.

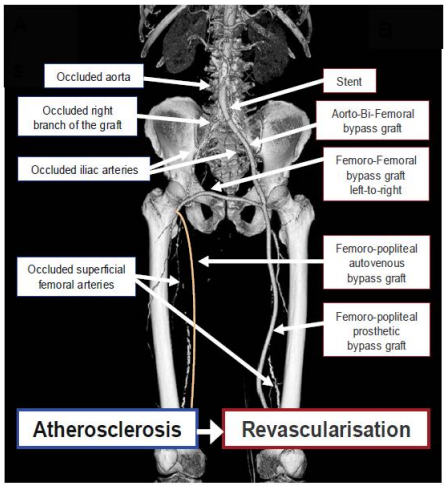

Figure 1-1: *Peripheral artery bypass procedures at different areas. Adapted from Chlupáč , Filová (5)*

1.1.2 Anatomy and Physiology of Blood Vessels

Blood vessels consist of a three-layered structure (Figure 1-2), namely; the tunica intima on the luminal side, lined with endothelial cells (EC) ; the tunica media in the middle, layered with smooth muscle cells (SMC) and elastin sheets; and the tunica adventitia on the outside, that consists of collagen fibres which protects, strengthens, and anchors the vessel (6). The EC layer is critical for gaseous and molecule exchange, preventing blood clotting and infection and inflammation of adjacent tissue, as well as controls the signal to a muscular component

of the tunica media (4). The SMCs in the tunica media is important for the dilation and contraction of the vessels during pressure changes, therefore the ECM, the spatial structure and arrangement of the EC and SMCs as well as the interaction between these two layers should be taken into careful consideration when designing vascular grafts (7).

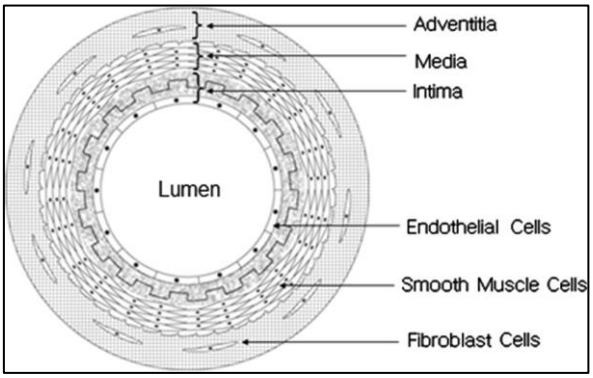

Figure 1-2: *Cross-section of an artery. Adapted from Hasan, Memic (7)*

1.2 Current Vascular Prostheses

1.2.1 Biological Vascular Grafts

Autologous vessel, such as the saphenous vein or the mammary arteries remain the paragon for vascular grafts but are unavailable in up to 20% of patients due to prior harvesting or other related diseases (8). Alternatives to autologous vessels are allografts (donor/cadaver), xenografts (bovine or porcine), and synthetic grafts (9).

Allografts are limited because of the shortage of tissue donors and/or anatomical variance, whereas xenografts have relatively short lifespans and poor control over physical and mechanical properties, as well as inflammation and calcification. Paediatric patients, acquiring a bovine or porcine xenograft, may require a new graft every 10-15 years (10-12). A summary of the biological vascular conduits in clinical use is represented in Table 1-1.

Table 1-1: Biological grafts as arterial and venous replacements. Adapted from Chlupáč , Filová (5)

	Biological vascular grafts			
	Autografts		**Allografts (homografts)**	**Xenografts (heterografts)**
	Arterial	**Venous**	**Arterial**	**Venous**
Advantages	Good diameter match, approximation and	Better availability and resistance to	Off the shelf availabilty, better infection resistance	
Disadvantages	Availability	Availability	Immunogenicity, graft dilapidation, occlusion, usual rejection, infection risk, constant drug intake	
Healing	Intimal hyperplasia	Dilation, intimal hyperplasia	Endothelial denudation, immune respone, fibrotisation	

1.2.2 Durable Synthetic Vascular Grafts

Two types of synthetic durable grafts have already been developed for commercial use: 1) polytetrafluoroethylene (PTFE) (Teflon and Gore-Tex), and 2) polyethylene terephthalate (PET) (Dacron and Terylene).

PTFE was patented as Teflon DuPont in 1937, and ePTFE (expanded PTFE) as Gore-Tex by Gore in 1969. ePTFE is favoured in medium diameter (6-12 mm) vascular prostheses when autologous vessels are not available. They are manufactured by a process which entails heating, stretching, and extruding producing a porous product with PTFE nodules (N) connected to oriented thin fibrils (F) as can be seen in Figure 1-3.

The surface of the ePTFE grafts is electronegative, due to the electronegative fluorine atom in the polymer, which minimises the reactions with blood components. The scaffolds have an average porosity between 30 – 90 µm which is described by the internodal distance (IND). The optimal IND of 60 µm (high porosity) was experimentally tested for tissue ingrowth and endothelialisation of a 4 mm ePTFE graft in a baboon model implant. Although the grafts showed capillary ingrowth in a human trial, it only extended half the distance, from the ablumen to the lumen, and did not produce an endothelial lining (13, 14).

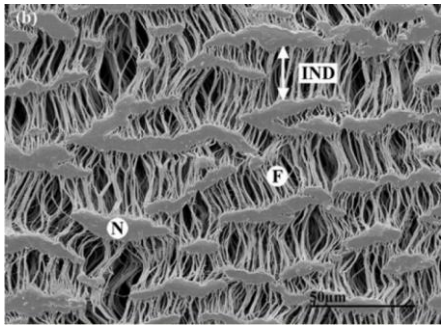

Figure 1-3: SEM image of an ePTFE vascular graft. Adapted from Pennel, Zilla (15).

PET is used to manufacture synthetic fibres of round cross-sections, consisting of multifilament bundled yarns, which are either woven (over-and-under) or knitted (looped) into textile vascular graft fabrics and tubes (Figure 1-4). The distensibility and kink-resistance are increased by using a crimping technique. Knitted Dacron is impregnated with collagen or gelatin to decrease the permeability, and to avoid the need for blood preclotting prior to implantation. Woven and knitted Dacron grafts have similar patency as an aorto-iliac bypass (16).

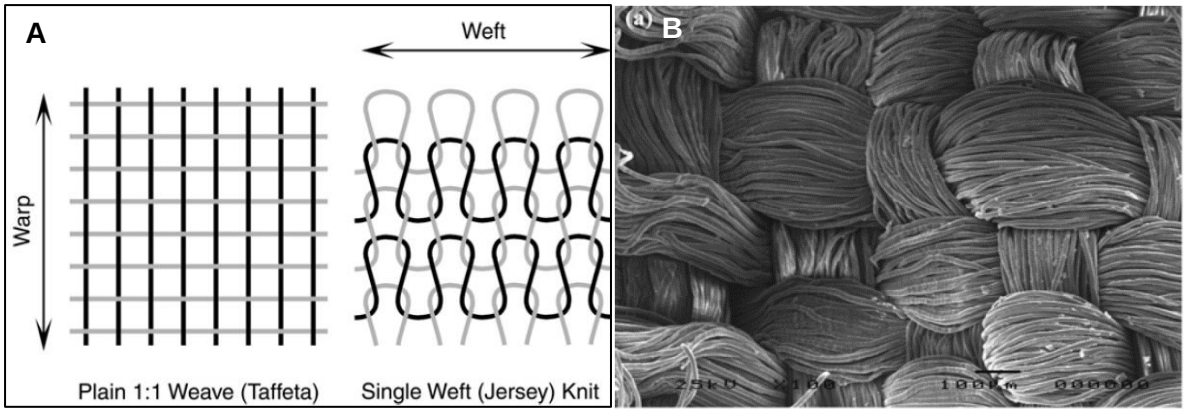

Figure 1-4: *A) Illustration of the woven and knitted pattern of a PET graft. B) SEM image of a woven Dacron vascular graft. Adapted from Pennel, Zilla (15).*

Polyurethane (PU) grafts are not commercially available but have been evaluated in clinical trials. Polycarbonate-based PU grafts promote faster endothelialisation and less intimal hyperplasia as a small diameter vascular prosthesis in a rat trial, compared to ePTFE (17). Poly(carbonate-urea) PU grafts showed a well-developed neointima at the distal anastomosis, with minor hydrolysis of the amorphous segments, and retained their compliance, after 36-month implantation in the aortoiliac position in dogs. The ePTFE and Dacron grafts did not retain their compliance (18). Table 1-2 is a comparison between the current commercial vascular grafts (PET and ePTFE) and an experimental PU graft.

Table 1-2: Synthetic vascular grafts (commercial and experimental). Adapted from Chlupáč , Filová (5)

	Synthetic vascular grafts				
	PET (Dacron, Terylen)		**ePTFE (Teflon, Gore-Tex)**		**Polyurethane**
	Woven	**Knitted**	**Low-Porosity (<30 µm IND)**	**High-Porosity (>45 µm IND)**	**Fibrillar**
Advantages	Superior stability, lower porosity, thus less bleeding	Higher porosity, better tissue ingrowth and compliance	Biostabe, no dilation	Biostable, superior cell ingrowth	Compliance, good hemo- and biocompatibility, better anti-thrombotic effect
Disadvantages	Low compliance, tissue ingrowth and porosity	Dilation, infection	Anastomotic bleeding, limited integration, infection	Neointimal delamination in 90 µm IND, infection	First generation had biodegradation, infection
Healing	Fibrin coverage at lumen, outer collagenous capsule, small clusters of endothelial cells	Fibrin coverage at lumen, small clusters of endothelial cells, transanastomotic endothelialisation in animals	Fibrin carpet at lumen, no transmural tissue ingrowth	Capillary sprouts, angiogenesis, intimal hyperplasia, endothelialisation in animals	Thin inner fibrin layer, limited ingrowth

1.2.3 Problems Associated with Current Prostheses

ePTFE has shown low patency rates (40-50%) in femoropopliteal reconstructions after 4 years, compared to the 70 – 80% of the reversed saphenous vein (19). Dilation is reported in Dacron grafts over time, however, direct complications and malfunctions are scarce(20).

Prosthetic rings or coils are applied to the surface of the PTFE and PET to elude kinking and compression in anatomically required positions. Evaluation of ePTFE and Dacron showed no evidence of one material being superior over the other (21). Currently, PET and PTFE are the only materials in use for commercial grafts, in an experimental setting PU grafts are showing promising results compared to PET and ePTFE.

It is possible for large diameter vascular grafts (> 6 mm) to overcome thrombosis due to the high blood flow, but small diameter grafts such as the peripheral and coronary arteries have limited long term patency (22). Small diameter synthetic grafts usually fail due to mid-graft thrombosis and/or intimal hyperplasia (Figure 1-5). These responses are usually due to the thrombogenicity of the material, compliance mismatches, inadequate biomechanical properties, and unsuitable diameters(19, 23).

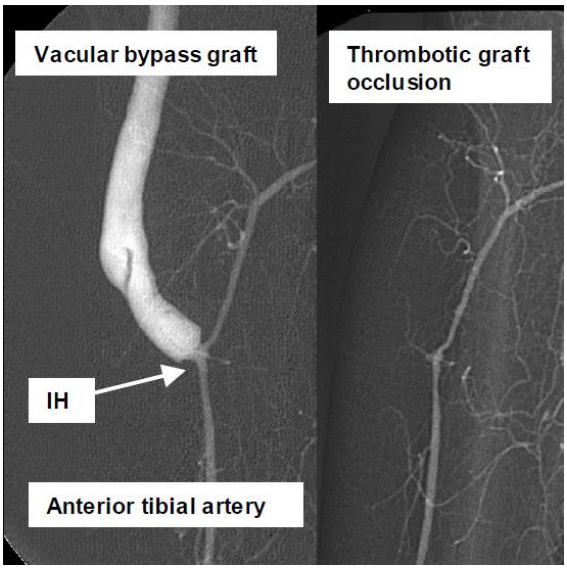

Figure 1-5: *Intimal hyperplasia at distal anastomosis. Adapted from Chlupåč , Filovå (5)*

1.3 The Concept and Application of Tissue Engineering

Tissue engineering offers a mean of creating vascular grafts by mimicking three-dimensional morphology of the extracellular matrix (ECM) while the polymer degrades, creating more space for the cells to form. Various ways have been developed to fabricate these vascular grafts for example; solvent casting-particulate leaching, molecular self-assembly, thermally induced phase separation, and electrospinning.

Total graft resorption with the avoidance of adverse foreign body reaction is a sought-after property of grafts. However, graft disintegration and embolisation of absorbed fragments through the lymphatic system remain a concern (24). Synthetic biodegradable conduits were first used when degradable and non-degradable materials were used to decrease the porosity of textile graft during implantation, without the sacrifice of increased porosity required for

healing (25). Degradation of the material occurs by means of hydrolysis of ester links, commonly based on lactic acid and glycolic acid, therefore the timing of degradation depends on the hydrophobicity of the polymer.

Hibino, McGillicuddy (26) produced a porous scaffold for the use of a vascular graft with a copolymer mesh of poly-L-lactide (PLLA) and poly-ε-caprolactone (PCL) strengthened with polyglycolide (PGA) and were seeded with autologous bone marrow-derived mononuclear cells (BM-MNCs) *in vitro* before implantation. The grafts remained patent although angioplasty was required in certain cases in 25 patients over a 7 year period (27). The scaffolds were completely degraded with the presence of vascular tissue, SMCs and endothelium on the lumen. However, these grafts were constructed for large diameter (12-24 mm) and were implanted in a high-flow, low-pressure system, which is lacking the results of small diameter (<6 mm) grafts.

Matsumura and Isayama (28) produced an acellular scaffold from a composite of knitted PGA and a copolymer poly(lactide/caprolactone) [P(LA/CL)] and poly(glycolide/caprolactone) [P(GA/CL)] sponge, in *vivo* in a canine model and showed patency for up to 1 year as a pulmonary artery replacement. Yokota, Ichikawa (29) did similar work on nonwoven PLLA and PGA scaffolds and showed patency for up to 1 year when implanted as a canine carotid artery.

1.4 Biomaterials and Bioactive Agents

1.4.1 Polyurethane

Polyurethanes have physical properties that can vary from soft and elastomeric to hard and rigid, while their chemical properties can also be chosen to improve durability and biostability (30). They consist of three different monomers: isocyanate (crystalline), polyol (amorphous), and a chain extender (31). The crystalline structure is usually the hard segment of the PU and the amorphous structure, soft. The ratios between the crystalline and amorphous sections can be varied with the chain extender to match the desired property. The elastomeric properties of certain polyurethanes make it an acceptable option for applications where interaction and mimicking of soft tissue are required (15). PU's are generally designed to be degradation resistant due to their hydrolytic and oxidative stability but by adding specific polyesters as the polyol, the polymer can be designed to be completely biodegradable.

1.4.2 DegraPol®

DegraPol® is a biodegradable polyester urethane, consisting of block copolymers shown in ***Figure 1-6***. The hard segment consists of poly((R)-3-hydroxybutyrate)-diol, the soft segment from poly(ε-caprolactone-*co*-glycolide)-diol and 2,2,4-trimethylhexamethylene diisocyanate as

the junction unit. The hard and soft segments are biodegradable with non-toxic degradation products (32). The mechanical properties can be varied with the ratio of hard to soft segments, while the degradation rate is increased by increasing the glycolide content in the soft segment.

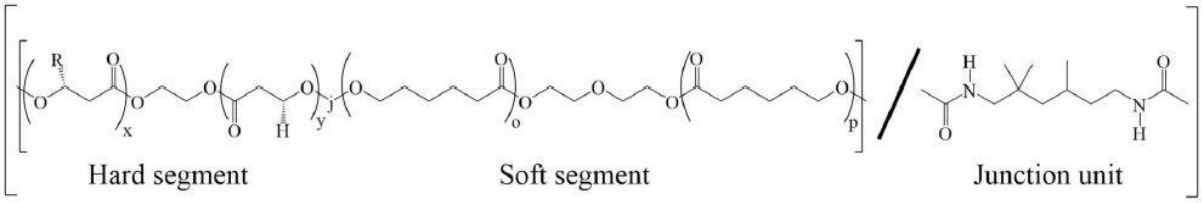

***Figure 1-6**: Degrapol® chemical structure.*

The version of DegraPol® used in this study (DP30) has a hard to soft segment ratio of 40:60 and a 70:30 ε-caprolactone to glycolide ratio (33). DegraPol® has been studied by various researchers as an electrospun tissue engineered scaffold for applications that include skeletal muscle, cartilage, tendons, drug delivery device, smooth muscles, and cardiovascular applications.

1.4.3 Heparin

Heparin is an anti-thrombotic substance, which naturally occurs on cellular surfaces and ECM (34). It is a highly sulphated and heterogenous polysaccharide, that is part of the glycosaminoglycans (GaGs) family and is either derived from a porcine intestine or bovine lung (35). The molecular structure consists of six different uronic acid and glucosamine linked disaccharides formed from ten monosaccharides. Heparin mainly interacts with the neighbouring proteins through electrostatic mechanisms, however, the formation of secondary structures, hydrophobic effects, and hydrogen bonding may occur, therefore it can bind to proteins such as specific growth factors (GFs), antithrombin, and lysozymes (36, 37).

GFs that have a natural liking for heparin include; vascular endothelial growth factor (VEGF) (38), platelet-derived growth factor-BB (PDGF-BB), (39), basic fibroblast growth factor (bFGF), and fibroblast growth factor (FGF-2) (40). Aside from heparin's anti-thrombotic properties, it is also able to control inflammation, promote cell adhesion, inhibit smooth muscle cell proliferation (41, 42) and stimulate angiogenesis (43, 44). These are all sought after properties to be included in the development of a tissue engineered vascular graft (TEVG) (45).

1.5 Applied Electrohydrodynamics for Tissue Engineering

1.5.1 Application of Electrohydrodynamics

Electrospinning offers a fabrication technique to develop scaffolds with fibre morphology that mimics that of the three-dimensional structure of the ECM (46). It makes it possible to vary the

mechanical properties and morphology of the TEVG. Polyurethanes are considered promising materials for TEVG's due to their superior mechanical properties and known biocompatibility (47, 48). TEVG's electrospun with polyurethane showed facilitation of *in situ* endothelialisation and proliferation, whilst leaving cell function unimpaired (49). However, the effects on cell migration *in vivo* are less commonly reported.

1.5.2 Electrospinning

1.5.2.1 Electrospinning Setup

Electrospinning normally comprises of a syringe filled with a polymer solution, pump, metallic needle tip, power supply, and collector (Figure 1-7). The polymer solution is pumped through the needle where an electric potential is applied to the solution. While the forces of the electric field increases, the spherical surface of the polymer solution elongates at the needle tip forming a conical shape known as the Taylor-cone (50). A jet of liquid accelerates from the Taylor-cone where it undergoes a bending instability rapidly whipping in expanding loops toward an oppositely charged and grounded collector (51). The whipping causes the elongation and thinning into the micro- and nanometer diameter fibres, while also undergoing solvent evaporation(52). Higher viscosity solutions will travel to the collector in a continuous jet and deposit as nanofibers, whereas lower viscosity liquids tend to break up and form droplets (electrospraying) (53).

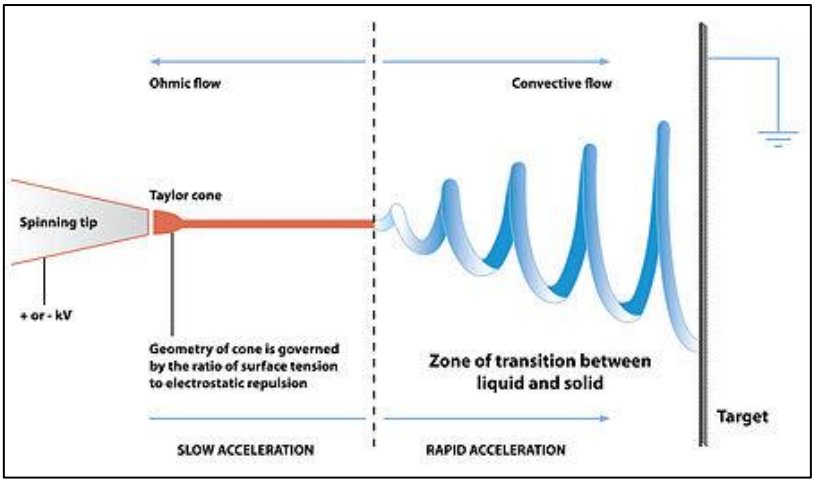

Figure 1-7: *Electrospinning process. Image: Joanna Gatford*

Various parameters can be varied to change the fibre morphology (fibre diameter, fibre orientation, pore size/porosity, and wall thickness) and mechanical properties (UTS, strain, Young's modulus, compliance) of the scaffold to match the native vessel's structure and function (7). These can be categorised into 3 main groups, namely; solution-, process-, and ambient parameters.

1.5.2.2 Solution Parameters

The solution parameters include polymer concentration, molecular weight, viscosity, surface tension, and conductivity/ surface charge density. The effect that the polymer concentration, viscosity, and surface tension have on the fibre morphology will only be discussed as these parameters are most commonly tuned to achieve the desired fibre morphology. The different effects that the polymer concentration has on the fibre morphology are listed in Table 1-3 and can be seen in Figure 1-8:

Table 1-3: Effect of polymer concentration on the fibre morphology in electrospinning.

Polymer Concentration	Effect on Fibre Morphology
Very low	Micro to nanoparticles.
Low	Mixture of bead and fibres (54, 55)
Suitable	Smooth micro- to nanofibers (54, 55)
Very high	Helix-shaped microribbons (56)

Sufficiently high solution viscosity is required to ensure that continuous smooth fibres are attained. Higher viscosity solutions tend to have smoother fibres due to the hard ejection of jets from the solution, whereas smooth fibres are difficult to attain from low viscosity solutions. The solution viscosity can be changed by varying the polymer concentration. It should be noted that the effect viscosity, polymer concentration, and molecular weight have on the fibre morphology are inter-related.

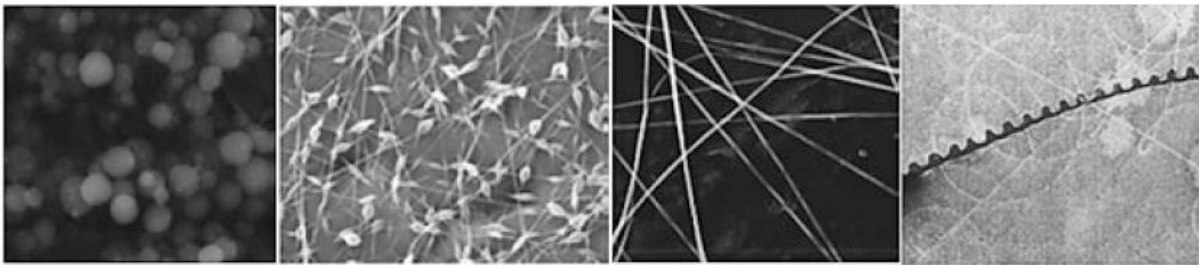

Figure 1-8: *SEM images of fibre morphology due to the effect of polymer concentration from very low (left) to high (right). Image adapted from Li and Wang (57)*.

The effect of surface tension on the fibre morphology was studied by Yang, Li (56) for electrospun poly(vinyl pyrrolidone) (PVP) with ethanol, DMF, and dichloromethane (MC) as solvents. The different solvents allowed for different surface tensions with the concentrations held fixed and smooth fibres were obtained with ethanol as the solvent, from previously beaded fibres with DMF and MC.

1.5.2.3 Processing Parameters

The process parameters are the applied voltage, flow rate, distance between needle tip and collector, collector size and rotating speed of collectors.

The applied voltage is an important factor in the electrospinning process, as a charged jet will be ejected from the Taylor cone only when the applied voltage is higher than the critical voltage (50). Each polymer-solvent system has its own optimum range of applied voltage (electric field strength) where nanofiber formation will occur. An applied voltage outside of this optimum range may result in beaded morphologies or completely inhibit polymer jet formation (53, 58).

Generally, the fibre diameter decreases with an increase in applied voltage beyond the critical voltage but increases at a certain point (59). The initial decrease in fibre diameter is due to the higher degree of jet stretching with an increase in charge repulsion within the jet and the strong electric field. The effect that the applied voltage has on the Taylor cone at the capillary was examined by Deitzel, Kleinmeyer (53) on a poly(ethylene oxide) (PEO)/water system. The variables were kept constant while only changing the applied voltage between 5.5-9.0 kV. An increase in the applied voltage increased the current and consequently led to an increase in the effective flow rate of the solution. The findings of the changes in the Taylor cone and the fibre morphology are summarised in Table 1-4.

Table 1-4: Changes in the Taylor cone and the fibre morphology with increased applied voltage.

Applied Voltage	Taylor Cone	Fibre Morphology
5.5	Jet ejected from apex.	Fibres free of defects.
5.5-7	Jet ejected from apex.	Few bead defects on fibres.
7	Jet ejected at capillary tip.	Beads more prevalent.
9	Jet ejected inside capillary tip.	Higher density of beads

As can be seen in Table 1-4 a minimum flow rate is required to maintain a stable Taylor cone, with an increase in voltage in order to replace the solution that is consumed when the solution is ejected from the jet. The flow rate has an influence on the fibre diameter, porosity, and geometry of the electrospun fibres. An increase in flow rate results in an increase in fibre diameter and porosity/ pore size due to the higher polymer volume available. If the flow rate is too high, beading defects may occur due to the solvent that does not have adequate time to evaporate (53, 60, 61).

1.5.2.4 Ambient Parameters

Although the ambient conditions in the electrospinning process are important for producing consistent scaffolds, its effect on fibre morphology has not been fully described in the literature.

The relative humidity plays an important role in fibre morphology of scaffolds, with Nezarati, Eifert (62) showing that the effects are dependent on the chemical properties (hydrophobicity) of the polymer and the solvent properties. The group investigated the effect of a relative

humidity (rH) range (5%-75%) on the fibre morphology with using PCU (hydrophobic) and PEG (hydrophilic). Low rH induced fibre breakage, whereas high rH induced nano-pores on the fibres for PCL and beading for PEG. PEG had increased film formation and fibre fusion due to water absorption and polymer dissolution, with PCU decreasing in fibre diameter as the excess water vapour facilitated electrostatic discharge and inducing jet stretching. De Vrieze, Van Camp (63) found that an increase in rH decreased the average fibre diameter of PVP (hydrophilic) up to a certain point where film formation occurs, the similar to results by Nezarati, Eifert (62) for the hydrophobic PCU. For a hydrophobic cellulose acetate (CA) it was found that an increase in rH increased the fibre diameter due to the fast precipitation of the CA, therefore prohibiting jet elongation. It is clear that the effect of rH on fibre morphology is still not fully understood, but it is clear that each polymer solution has its own optimal rH for electrospinning.

1.6 Electrospun Tissue Engineered Vascular Grafts

1.6.1 Function and Properties of Vascular Grafts

The vascular graft should be able to withstand the flow of blood without leakage and the associated pressure changes. It should have similar compliance and geometry than that of the native vessels to prevent high-stress areas around the anastomosis and induce undesirable flow characteristics (64-66). This disruption in blood flow causes recirculation zones, flow separation, and low wall shear stress (67), which results in vasoactive substances, gene activation, protein expression, and cytoskeletal rearrangement that stimulates neointimal hyperplasia (68). The TEVG should be able to withstand a burst strength above 260 kPa and have similar mechanical properties as the native vessel, listed in Table 1-5 (69). It is also required that the TEVG provide an anti-thrombotic lumen and sufficient porosity to mimic the ECM of the native vessel.

Table 1-5: Mechanical properties of some native blood vessels. Adapted from Stekelenburg, Rutten (70)

Blood vessel	Elastic	Ultimate stress	Strain at	Burst strength
SV* (circ.)	4.2	1.8	242	1680-3900
SV (long.)	23.7	6.3	83	-
LIM (circ.)**	8	4.1	134	2000
LIM (long.)	16.8	4.3	59	-

*SV – Saphenous vein, **LIM – Left internal mammary artery, circ. – circumferential, long. - longitudinal

1.6.2 Electrospun TEVG's

The fibrous structures obtained by electrospinning grafts are designed to mimic the soft tissue structure of the ECM as shown in Figure 1-9.

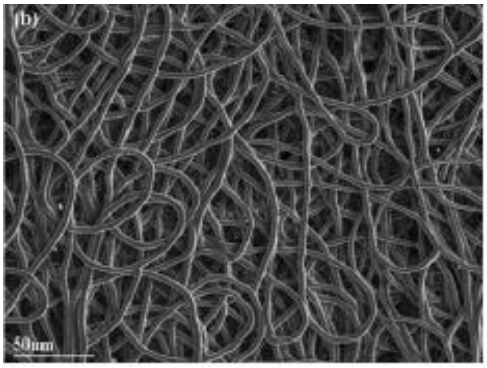

Figure 1-9: *SEM image of an electrospun PU vascular graft. Adapted from Pennel, Zilla (15).*

Various polymers have been used in the electrospinning process for the manufacturing of grafts with blends of PU, styrenated (ST)-gelatin and type I collagen, as well as PU and polyethylene oxide (PEO), and poly (D, L-lactic-co-glycolide) (PLGA). The PLGA with elastin and type I collagen composite graft showed superior biocompatibility with favourable tissue composition and mechanical properties (71). Poly ε-caprolactone (PCL) was also used to fabricate 3 mm electrospun grafts with collagen, PEO, or gelatin, or Heprasil, and showed improved attachment and proliferation of human fetal osteoblasts (72).

A multilayer structure was electrospun by Soletti, Hong (73) with biodegradable poly(ester urethane) urea (PEUU) and thermally induced phase separation (TIPS). Vaz, van Tuijl (74) fabricated a bilayer structure of a circumferentially aligned fibrous PLA outer layer with a randomly oriented elastic PCL inner layer.

He, Ma (75) produced acellular tubular poly-L-lactic acid-co-poly-ε-caprolactone (PLL-CL) grafts of 3 mm diameter. After a 7 week in *vivo* study in rabbits, the structure of the grafts was preserved and was patent.

Kwon and Matsuda (76) produced an elastomeric nanofiber fabric with coaxial electrospinning, from equimolar copolyester, poly(L-lactide-co-ε-caprolactone) (PLCL), with type I collagen or the tri-*n*-butylamine salt of heparin (heparin-TBA) using HFIP as a solvent. Yin, Luo (77) successfully produced a 4 mm vascular graft from collagen/chitosan/PLCL and heparin. Heparin is a known anti-coagulant that also inhibits smooth cell proliferation, reduce inflammation and control angiogenesis, which are useful properties in aiding with thermogenesis and intimal hyperplasia (42, 78, 79).

The heparin presented with a sustained release for more than 45 days in *vitro* and possessed suitable mechanical properties to match those of a native blood vessel. The core-shell structure of the fibres, as well as the SEM images of the vascular graft, can be seen in Figure 1-10.

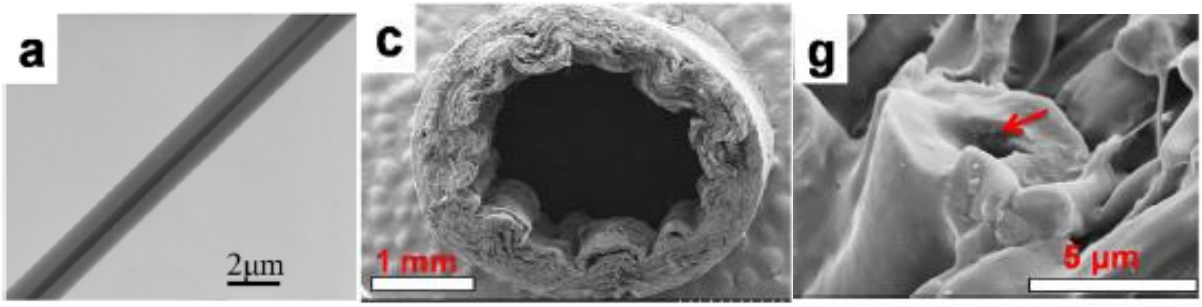

Figure 1-10: *a) TEM image of fibre with core-shell structure, b) SEM image of the cross-sectional view of the conduit, c) high-resolution image of fibre cross-section. Adapted from Yin, Luo (77).*

An acellular biodegradable TEVG was designed by with poly(glycerol sebacate) (PGS) by a modified salt fusion and leaching method for improved porosity and coated with heparin. The graft was wrapped with a 15 µm electrospun PCL sheath to increase the mechanical and suture strength (Figure 1-11). The mechanical properties of the grafts were also similar to native arteries. The ID of the graft was measured as 720 µm with a wall thickness of 290 µm. In *vivo* evaluation was done on rats as an interposition graft in the abdominal aorta for 3 months.

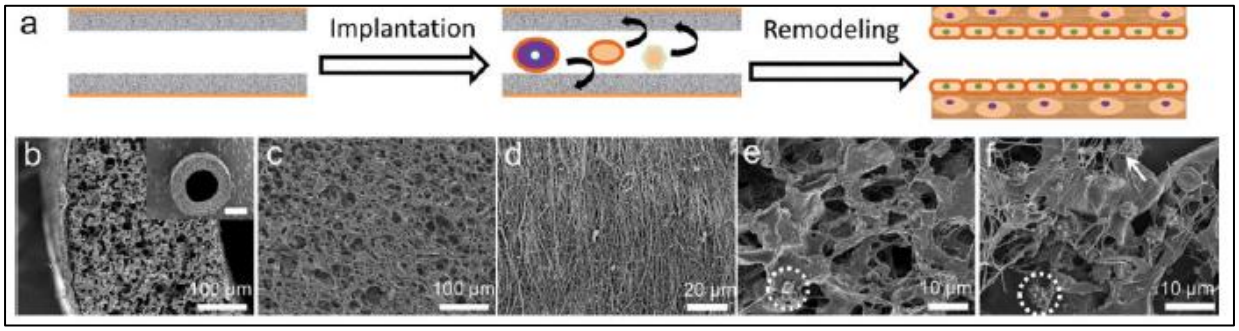

Figure 1-11: *a) Schematic representation of the proposed remodelling process.SEM images of: b) composite graft. c) Lumen. d) PCL sheath. e) PGS (heparinised) after incubation in platelet-rich plasma (PRP). f) PRP incubated unheparinised PGS.*

The explants resembled neo-arteries with synchronous pulsation, full endothelialisation and contractile SMCs, co-expression of elastin, collagen, and glycosaminoglycan, with good mechanical properties (Figure 1-12). Although the PCL improved the suture strength of the graft, constituents of the graft were observed at 3 months and are likely to be PCL, because PGS degrades within 2 months subcutaneously (24).

PEUU acellular grafts were implanted by Soletti, Nieponice (80) in adult rat models as aortic interposition grafts for up to 24 weeks. The lumen of the grafts was coated with a non-thrombogenic 2-methacryloyloxyethyl phosphorylcholine copolymer. The coated grafts have decreased platelet adherence and improved patency as compared to the uncoated PEUU grafts. A summation of *in* vivo circulatory model studies conducted is presented in Table 1-6.

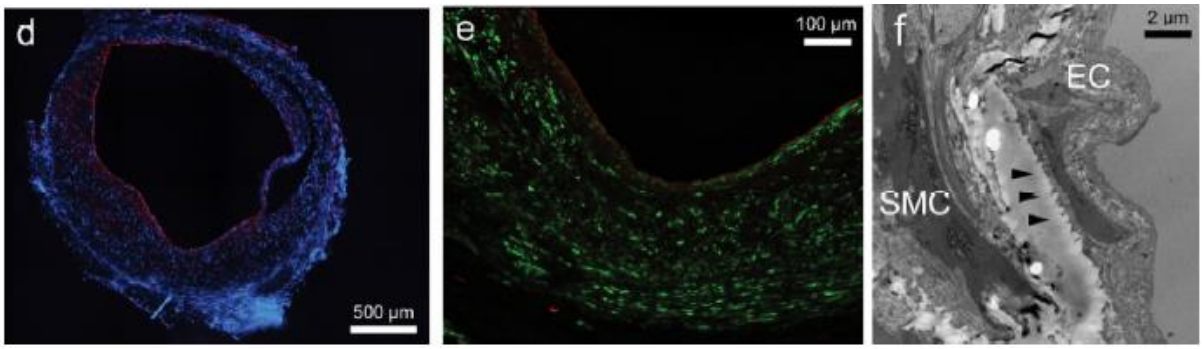

Figure 1-12: *d) Endothelium (EC) on lumen (red). Nuclei counterstained (blue). e) Endothelium distribution (red) and smooth muscle cells (SMC,green). f) TEM image of EC/SMC interface. Arrowheads indicate a basement membrane.*

Milleret, Hefti (81) compared the effects of fibre diameter and surface roughness of electrospun scaffolds on blood activation between DegraPol® (DP) and PLGA. No differences were found between the DP and PLGA with similar topographies but the scaffolds with thin fibres (<1 µm) triggered low coagulation and almost no platelets adhered. Evrova, Houska (82) and Meier Burgisser, Calcagni (83) have shown that electrospun DP is a suitable choice for drug delivery in the healing of a tendon rupture repair and the prevention of peritendinous adhesions of rabbits. However, good results were obtained, no studies have been done on the circulatory model for DP.

1.6.3 Challenges of Electrospun Vascular Grafts

Hufnagel (84) implanted solid, rigid, polymeric poly(methyl methacrylate) tubes and were unsuccessful due to their impervious nature. This finding indicated that porosity was a necessity for cellular ingrowth, as showed by Wesolowski, Fries (25) with their successful porous polymer prosthesis, compared to their unsuccessful solid-walled prosthesis. This led to the findings of Voorneveld, Oosthuysen (85) were high porosity polyurethane scaffolds had increased vascularisation than low porosity scaffolds in an in *vivo* subcutaneous study on male Wistar rats. It is generally agreed that porosity is a crucial factor in the design of the vascular grafts although the nature and dimensions of the porosity required are not known for proper healing.

Vascular endothelium on the luminal surface is critical toward the non-thrombogenic character and patency of vascular grafts. Endothelium originating from the anastomosis of an adjacent artery on the luminal surface has been well documented, however, this trans-anastomotic ingrowth is usually only 1–2 cm from either anastomosis (86-88). Mid-graft endothelialisation has been shown with isolated transmural endothelialisation with high-porosity grafts, independent of the transanastomotic ingrowth without an increase in intimal hyperplasia (89). Most of these constructs have not been tested in *vivo*, therefore their performance needs to be assessed in animals and clinical settings.

Table 1-6: *In vivo* circulatory model assessment of studies done with electrospun vascular grafts. Adapted from (90)

Polymer	ID (mm)	Length	Animal Model	Dur	FB	Modification/Comments	Reference
PLLA	0.7	-	Rat (CCA)	7.5	0.5	MSC seeded	(91)
PCL	2	13	Rat (AA)	24	1,9		(92)
PCL	2	13	Rat (AA)	12	1,9		(93)
PCL	2	-	Rat (AA)	24	1,6	Paclitaxel surface mod	(94)
PCL: Collagen (1:1)	4,75	40	Rabbit (AIB)	4	0,52		(95)
PCLA	1	10	Rabbit (EGV)	7	0,5	Collagen coating	(75)
PEUU:PMBU (85:15)	1,3	10	Rat (AA)	8	0,5		(96)
PEUU	1.2	10	Rat (AA)	8	-	Outer layer electrospun, inner	(97)
PLLA	1	7	Rat (CCA)	26	2	Hirudin surface mod	(98)
Elastin + PCL sheath	2,8	20	Rabbit (CCA)	4	1,6		(10)
PEUU	1,3	10	Rat (AA)	8	1	PMA surface mod	(80)
PCL	2	10	Rat (AA)	78	2,2		(99)
PCL	2	20	Rat (AA)	12	2,2/0,8	Bilayered, H/L Por 83%/ 65%, PS	(100)
PCL	0,7	7	Rat (CCA)	6	-	CAG surface	(101)
PGS/PCL	0.72	-	Rat (AA)	12	-	Salt leaching inner layer-PGS,	(24)
PCL	2,2	15	Rabbit (CCA)	4	3	RGD surface mod	(102)
PCL	2	40	Dog (FA)	4	-	Por 83, Heparin surface mod	(103)
Pellethane ®	1,5	15	Rat (AA)	26	0,88	-	(104)
PCL/chitozan/pNSR32	1,2	15	Rat (AA)	8	-	-	(105)
PCL + PU layer	2,5	40	Dog (FA)	8	0,5/ 0,2-1,0	Por 49%, Heparin surface mod	(106)
Coaxial PCLA	2,5-3,5	50	Dog (FA)	4,5	-	Heparin core	(107)
Coaxial PCLA	4	50	Dog (FA)	24	<1	Heparin core, EC seeded	(108)
Coaxial PCLA	4	50	Dog (FA)	24	0,3	Heparin core, EC seeded	(109)
PU	1,5	15	Rat (AA)	26	1,0/0,9	H/L Por 80%/ 53%, PS 4 µm/	(110)
TPU	1,6	20	Rat (AA)	52	1,4	Por 75%, PS 4,7 µm	(111)

ID = internal diameter of vascular graft, FD = fibre diameter, Dur – duration, H = high, L = low, Por = porosity, PS = pore size PLLA = poly(l-lactic acid), PCL = poly(ε-caprolactone), PCLA = poly(ε-caprolactone-co-L-lactic acid), PEUU = poly(ester urethane)urea, PMBU = poly(2-methacryloyloxyethyl phosphorylcholine-co-methacryloyloxyethyl butylurethane), PGS = poly(glycerol sebacate), PU = polyurethane, PMA = 2-methacryloyloxyethyl phosphoylcholine, CAG = Cysteine-alanine-glysine trimer peptide, RGD = arginine-glycine-aspartic acid, MSC = mesenchymal stem cells, EC = endothelial cells, CCA = common carotid artery, AA = abdominal aorta, FA = femoral artery, AIB = aortoiliac bypass, EGV = inferior epigastric vein

1.7 Project Aim and Objectives

This study aims to produce a small diameter biodegradable vascular graft (Degrapol®, DP30) with sufficient porosity/pore size and incorporate heparin as a potential angiogenic/anti-thrombotic agent for rapid transmural ingrowth of cells.

The objectives of this study were to:

- Modify and upgrade the existing electrospinning unit.
- Design and build a humidity control unit for the electrospinning rig.
- Determine the influence of rH and solvent system used on the fibre morphology and mechanical properties of the electrospun scaffold.
- Incorporation of HepTBA in the electrospun fibres by means of blend electrospinning.
- Evaluate the *in vitro* heparin release from the scaffold.
- Evaluate the change in mechanical properties, by means of a degradation study, and fibre morphology with the addition of HepTBA to the electrospun grafts.
- Evaluate the *in vivo* healing response of the inclusion of HepTBA in the DP30 scaffold in a pilot study with a rat infrarenal aortic model.

2 Materials and Methods

This chapter provides information on the materials and methods used in the development of a biodegradable electrospun vascular graft. The sections discussed will be the design of the electrospinning rig and humidity control unit, the relative humidity (rH) and solvent system parametric study, graft morphology characterisation, mechanical properties characterisation, heparin incorporation, *in vitro* heparin release, and the degradation study. Thereafter, the pilot study evaluating the *in vivo* performance of the electrospun vascular graft with their respective histological analyses.

2.1 Materials

The biomaterial chosen for the development of the electrospun vascular grafts was DegraPol30® (DP30, 1.15 g/cm^3, ab medica, S.p.A, Lainate, Italy). All reagents and solvents were purchased from Fluka (Buchs, Switzerland), Merck Millipore (RSA), Oakwood Chemical (USA), Saarchem Holpro Analytic (RSA), and Sigma-Aldrich (Pty) Ltd. (RSA) unless stated otherwise. Heparin sodium was obtained from Celsus Laboratories (USA).

2.2 Electrospinning

2.2.1 Polymer solution preparation

All electrospinning solutions were prepared by magnetic stirring overnight at RT, using glass test tubes or bottles (Pyrex®), depending on the volume. After stirring the solution was left for an hour to remove bubbles and equalise the minimal heat generated through stirring, before transferring to a syringe for processing. The solution concentrations were expressed as a weight-by-weight percentage (%wt/wt) for the mass of polymer to the mass total solution unless stated otherwise.

2.2.2 Experimental setup

The experimental setup for the TEVG consisted of a custom-built rotation and translation stage with adjustable speed settings(Figure 2-1) and a humidity control unit (Figure 2-2). The following equipment was used for the electrospinning rig:

- Two high voltage power supplies, one positive and the other negative in polarity (ES30P-5W/ES30N-5W, respectively, Gamma High Voltage Research, USA).
- Syringe pump (SE400B, Fresenius, Bad Homburg, Germany).
- 6 cm x 6 cm stainless steel base plate.
- 21 G blunted needle.
- Syringes (B Braun, Germany).
- 0.067” stainless steel 304V rod (Small Parts Inc., Logansport, USA).

The syringe pump was used to feed the polymer solution to the blunted needle (via tubing), connected to the base plate and was charged positively with the power supply. The negative power supply was connected to the mandrel while rotating at a set speed. The translation and rotational speed were controlled with an Arduino Mega 2560 micro-controller. The rotational speed, translation speed, polymer solution flow rate and distance from needle tip to collector were set to optimum conditions, determined by initial trials and requirements.

2.2.3 Design of electrospinning rig

Figure 2-1 is an illustration of the electrospinning rig to control the process and ambient parameters to obtain the desired fibre morphology and mechanical properties for the electrospun vascular graft.

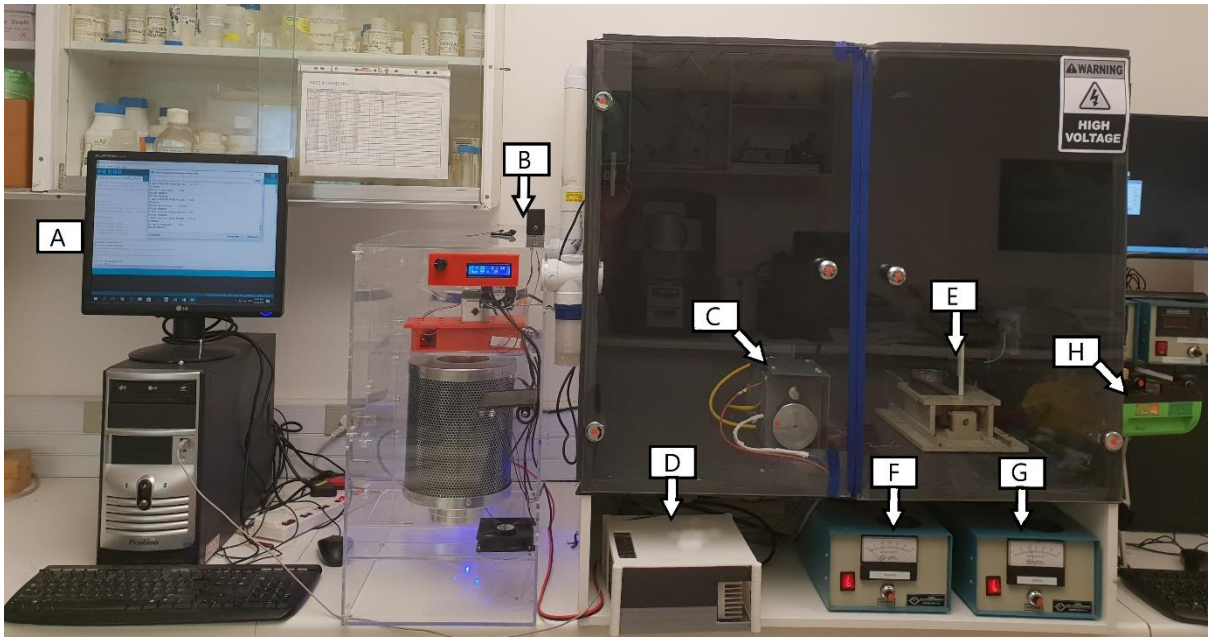

Figure 2-1: *Electrospinning set-up. (A) Serial monitor for rotation and translation speed input. (B) Environmental control unit. (C) Mandrel stage. (D) Arduino Mega 2560 micro-controller unit for rotation and translation speed. (E) Negative power supply. (F) Positive power supply. (G) Negative power supply. (H) Syringe pump.*

2.2.3.1 Design of electrospinning unit (processing parameters)

The design of the electrospinning unit consisted of two NEMA stepper motors (23HSX-102, 12 V, 1 A, Blantech Technology Supplies, RSA, and RS Pro 191-8362, , 12 V, 0.6 A, RS Components, UK, respectively) to control the rotational speed, translation distance, and translation speed (processing parameters), connected to a driver (G203V stepper drive, Geckodrive, USA) that was controlled with an Arduino Mega 2560 micro-controller (Communica, RSA). The hardware was powered by a power supply (8A, 12V, Communica, RSA).

The Arduino Mega 2560 was programmed (Process_Parameters_Control.ino) to receive inputs (rotational speed in RPM, translation speed in mm/min, and translation distance in mm) from the serial monitor (Figure 2-1A) and use that as the output for the stepper motors (Figure 2-1C and Figure 2-1D). The Arduino Mega 2560, Gecko drivers, and power supply was safely stored in a 3D printed box (Figure 2-1D). The rotational stage and translation stage were kept inside a melamine cabinet with sealed glass doors, to ensure that there is no interference from the environment. The inside of the box was painted black to improve the visibility of the fibre jet.

2.2.3.2 Design of humidity control unit

The humidity of the electrospinning chamber was controlled using an environmental control unit custom built for this purpose (Figure 2-1B, Figure 2-2). This unit consisted of an activated carbon filter (Figure 2-2B, Advanced Air Carbon Filter, 4”x12” size, 200 CFM flow rate, Futurama, RSA) for the removal of the solvent vapour, a filter filled with desiccant silica gel for removing moisture from the air (Figure 2-2-1D), a nebulizer (Figure 2-2-1D and 2B, NB-80E-01-H, TDK Corporation, Digi-Key, USA) to increase the relative humidity, a humidity sensor (Adafruit SHT31-D, Communica, RSA), which is controlled by an Arduino Uno micro-controller (Humidity_Control.ino, Communica, RSA). The LCD screen (16x2, IIC/I2C/TWI, Communica, RSA) displays the temperature (°C), relative humidity (rH%), and desired relative humidity set point inside the electrospinning chamber (Figure 2-2-2A). The hardware was powered by the same power supply mentioned in Section 2.2.3.1 Design of electrospinning unit (processing parameters).

The air flow of the unit was directed by 3 separate high-speed fans (10cmx10cm, 12 VDC, 0.35 A, Communica, RSA) controlled by the Arduino Uno. Figure 2-3 illustrates the different flow configurations, where the white arrows indicate the inlet flow through the activated carbon filter, the red arrows indicate the drying loop (desiccant), and the blue arrows indicate the wetting loop (nebulizer). When the set point was reached, the flow followed the direction of the white and blue arrows and the nebulizer switched off by the micro-controller.

Testing of humidity control unit: The efficacy of the humidity control unit was tested by simultaneously measuring the ambient relative humidity (rH) and the rH inside the chamber. The drying and wetting loop was tested by choosing a set point of 30%, thereafter it was changed to 5% rH above the ambient rH and readjusted to an arbitrary set point of 35% rH. The unit was run for 30 min at each set point with the chamber sealed to ensure that there was no assistance on the change in rH by the ambient rH.

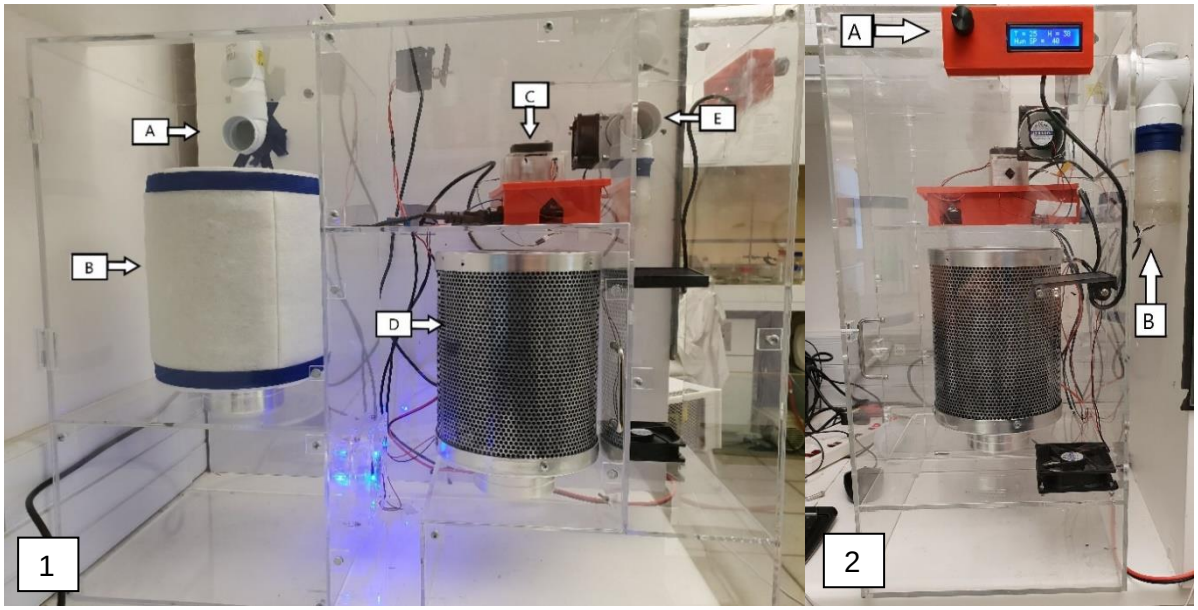

Figure 2-2: *Environmental control unit side view (1) and front view (2). (1A) Inlet. (1B) Activated carbon filter. (1C) Arduino Uno micro-controller unit. (1D) Desiccant drying loop. (1E and 2B) Outlet and nebulizer (wetting). (A) Adjustable setpoint control, relative humidity setpoint-, actual relative humidity-, and temperature display.*

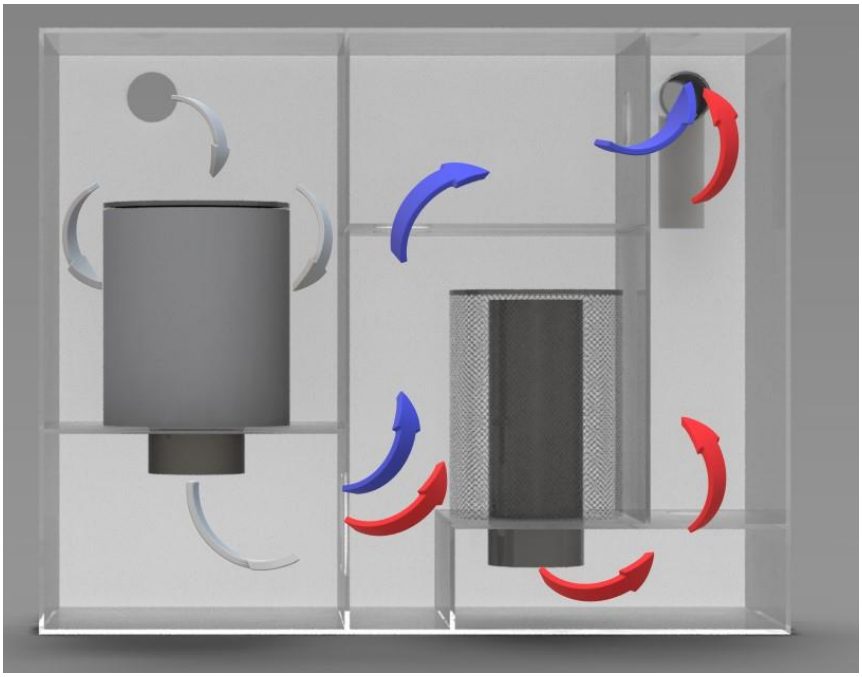

Figure 2-3: *Flow illustration of the humidity control unit. White arrows indicate normal operating flow at set point, blue arrows indicate the wetting loop and red arrows indicate the drying loop.*

2.2.4 Electrospinning parameters

After the initial pilot studies and experimentation, the parameters used throughout the study are listed in Table 2-1.

Table 2-1: Parameters used throughout the study for electrospinning

Parameter	Value
Polymer concentration	24% w/w
Flow rate	2 mL/h
Mandrel rotational speed	150 rpm
Translation speed	2 mm/s
Translation distance	10 cm
Collecting voltage	-5 kV
Baseplate size	6 cmx6 cm
Needle size	21G

2.2.4.1 Solvent system and humidity parametric study

The solvent system and humidity were chosen for the optimisation of the electrospun vascular grafts. The input parameters are listed in Table 2-2.

Table 2-2: Parametric studies

Solvent (w/w)	Polymer conc (% w/w)	Distance (mm)	Humidity (% rH)	Mandrel diameter (mm)	HepTBA conc. (% w drug/ w polymer)	Applied voltage (kV)
Parametric study for optimisation of the solvent system and humidity.						
Pure chloroform (n = 4)	24	300	30, 40, 50	2.1		15
99% Chloroform, 1% HFIP (n = 4)	24	300	30, 40, 50	2.1		15
95% Chloroform, 5% HFIP (n = 4)	24	300	30, 40, 50	2.1		15
Grafts for *in vitro* analysis						
Pure chloroform (n = 3)*	24	300	30	1.7	-	11
Pure chloroform (n = 3)*	24	300	30	1.7	3	7
Pure chloroform (n = 3)	20	300	30	1.7	5	7

*Parameters chosen for the manufacturing of the grafts for the *in vivo* pilot study

2.2.4.2 Grafts for *in vitro* analysis

An acute animal study (protocol 016-021) was done, to test the handling and fit of the grafts on an infrarenal aortic model on the available male Wistar rats. Based on the outcomes of the study it was found that the ID (2.1 mm) was oversized for the site of animals available at the time and the ID of the grafts was changed accordingly (1.7 mm). Heparin was incorporated in these grafts as described in section 2.5 ‘Heparin incorporation’, and can be seen in Table 2-2.

2.2.4.3 Grafts for *in vivo* pilot study

The parameters chosen to manufacture the grafts for the *in vivo* pilot study (protocol 018-038) are shown in Table 2-2 marked by an **asterisk (*).**

2.3 Characterisation of graft morphology

2.3.1 Scanning electron microscopy

The dry samples were cut and placed on metal stubs (to view the lumen, ablumen, and the cross-section) and sputter coated with gold (120 s, 35 mA, 1.4 V, Polaron SC7640, Quorum Technologies, England). The images were acquired with an FEI NovaNano Scanning Electron Microscope (SEM, 20 keV).

2.3.2 Fibre diameter, pore size, and orientation

ImageJ (version 1.51k), with the plugin 'DiameterJ', was used to measure the fibre diameter, pore size, and fibre orientation (112). This plugin gave the data in the form of a .csv file as an output.

Briefly, images taken from the SEM were cropped, put in the same folder, and then segmented with the DiameterJ Segment plugin with 'Stat. Region Merged' and 'Mixed' chosen for the segmentation algorithm. The best-segmented image of each SEM image was chosen (Figure 2-4) and analysed with the DiameterJ .1-018 plugin. A guideline of the ideal segmented image is shown in Figure 2-5.

The DiameterJ 1-1018 plugin was run with the following settings; orientation analysis (OrientationJ), convert pixels to real units (yes), length of scale bar (207 pixels, may vary), length of scale bar (50 microns), identify location of specific radius (no), min fibre radius (1 pixels), max fibre radius (255 pixels), analyse more than one image (yes), and combine analysis from all images with DiameterJ (yes). The length of scale bar (in pixels) was determined by zooming onto the scale bar and then selecting the 'straight' line function in ImageJ and drawing a line that spans from the one end of the scale bar to the other end. The length of the scale bar (in pixels) will appear under the toolbar of ImageJ.

The OrientationJ Measure (No pre-filter, Ellipse thickness: 0.5, Ellipse opacity: 100, Ellipse colour: 255:0:0, Area opacity: 50, Area colour: 128:128:0) plugin runs simultaneously with the DiameterJ 1-018 plugin by selecting "OrientationJ" from the drop-down menu under the "Orientation Analysis" section. The Orientation Index (OI, $0 \leq OI \leq 1$) quantifies the fibre alignment of each graft, where an OI of unity (1) represents perfect fibre alignment and an OI

approaching zero (0) indicates more randomly aligned fibres. Figure 2-6 A and Figure 2-6 B shows an example of an OI of 0.2 and 0.96, respectively.

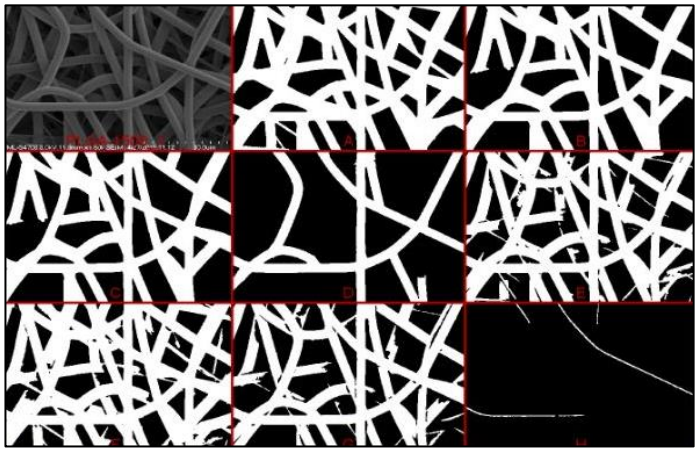

Figure 2-4: *Montage of different segmentation algorithms used.*

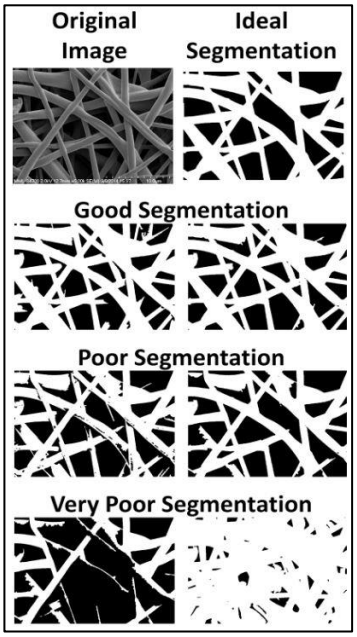

Figure 2-5: *Guideline of the ideal segmented image.*

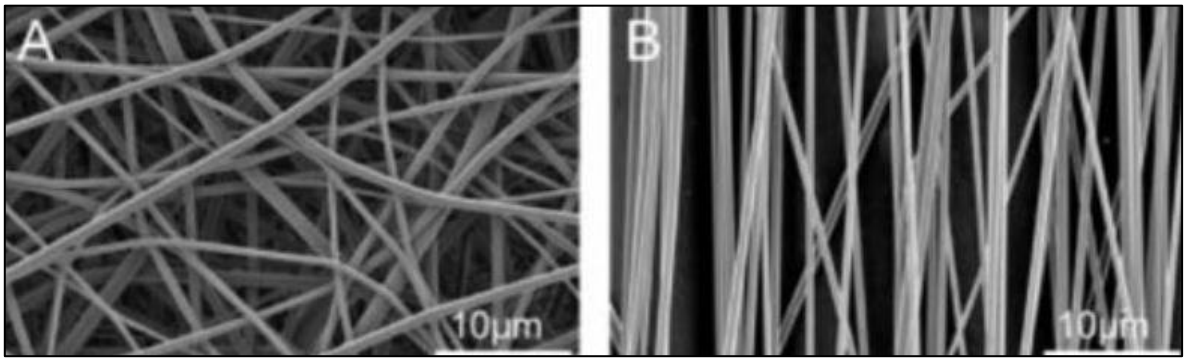

Figure 2-6: *(A) Randomly aligned fibres. (B) Aligned fibres (113).*

The fibre diameter, pore size and, fibre orientation were determined for the lumen and ablumen with a sample size of n = 4 for each group (4x2 images per group).

2.3.3 Porosity

The porosity of the graft, P, is defined by Equation 1. As direct measurement of these quantities is not feasible, Equation 2 was derived from Equation 1 as described and used by many others (114-116). These quantities were determined by means of hydrostatic weighing, using a lab balance scale ((XS105S analytical balance; Mettler Toledo, Greifensee, Switzerland, Adam), by weighing a graft, 10 mm in length, a) in air (Figure 2-7A) and b)

submerged in ethanol (Figure 2-7B), eliminating all air from the graft (AAA250L analytical balance with Adam density determination kit, Adam Equipment Inc, Danbury, CT, USA).

$$P = 1 - \frac{V_{fibres}}{V_{total}} \quad \textbf{(1)}$$

$$P = 1 - \frac{m_{s,air} - m_{s,eth}}{\rho_{eth} V_{total}} \quad \textbf{(2)}$$

Where $m_{s,\,air}$ and $m_{s,\,eth}$ are the mass of the sample in air and mass of the sample submerged in ethanol.

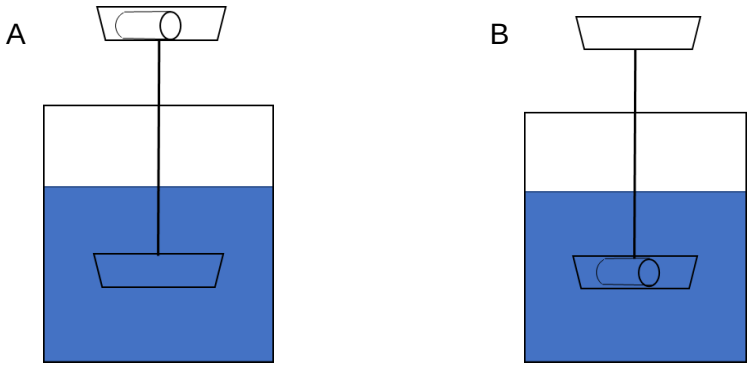

Figure 2-7: *Hydrostatic weighing A) in air and B) in ethanol*

2.4 Mechanical characterisation

All samples were tested in the longitudinal and circumferential direction, submerged in a phosphate buffered saline (PBS) at 37 ± 2°C, using a tensile tester (Instron 5544, 10N load cell, Norwood, USA).

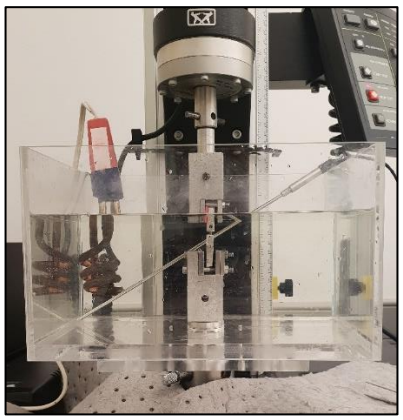

Figure 2-8: *Instron set-up for tensile testing under simulated physiological conditions.*

The ultimate tensile strength (UTS) and maximum elongation (ε_{max}) were defined as the stress and strain at the point of global maximum stress on the stress/strain curve, whereas Young's modulus (E_y) was approximated as the 10% secant modulus. The samples were tested until failure at a strain rate of 66 mm/min, based on the compliance of a healthy blood vessel

(8%/100 mmHg) and a heart rate of 72 bpm (117, 118). The sample size tested for the different groups are listed in **Table 2-3**.

Table 2-3: Sample size for the different groups* tested.

Graft internal diameter (mm)	Sample size (n)
2.1	4
1.7	3

*The groups include all the different solvent systems and rH used, as well as drugs incorporated for the specific mandrel.

2.4.1 Longitudinal tensile testing

The electrospun samples (30 mm, 10 mm gauge length) were clamped in a tensile tester, with custom-made stainless-steel clamps with diamond patterned rubber grips (Figure 2-9). The wall thickness of the sample was measured with a calliper.

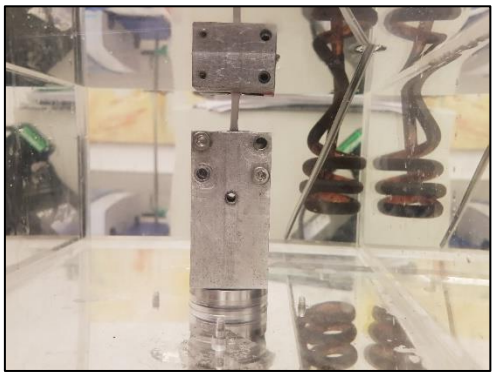

Figure 2-9: *Longitudinal tensile testing of electrospun vascular grafts.*

The force-displacement data was logged and imported into Python, where it was processed as stress-strain plots. The UTS, ε_{max}, and E_y were determined with a custom Python script and exported to an Excel workbook.

2.4.2 Circumferential tensile testing

2.4.2.1 UTS – Hoop stress

The vascular grafts were tested in the circumferential direction with a custom-made device until failure at a strain rate of 66 mm/min (Figure 2-10c). The sample (5 mm width) was held by two pins (1 mm OD, Figure 2-10a) and then stretched, such that the graft walls were near parallel but measured a load that is less than 0.01 N (Figure 2-10b). The wall thickness was measured with a calliper.

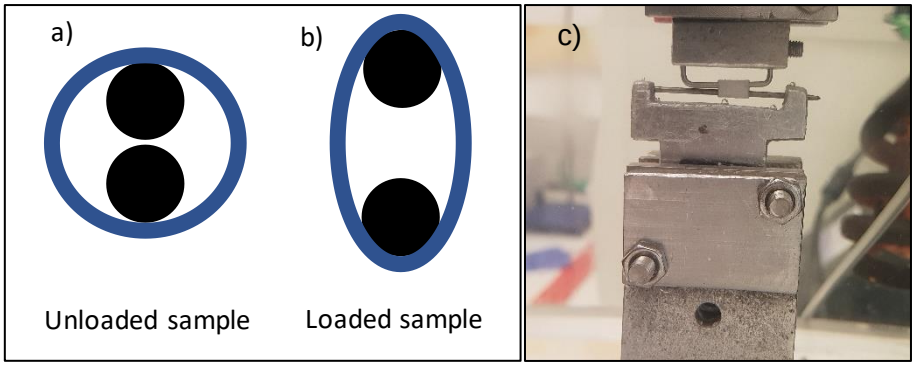

Figure 2-10: *Circumferential tensile testing. a) Unloaded sample held by pins. b) Loaded sample held by pins. c) Set-up in on Instron tensile tester.*

The force-displacement data was logged and imported into Python, where it was processed as a stress-strain curve. The hoop stress was calculated with Equation 3.

$$\sigma_{hoop} = \frac{F}{2 \cdot t \cdot w} \quad \textbf{(3)}$$

Where σ_{hoop}, *F, t,* and *w* are the hoop stress (MPa), force (N), wall thickness (mm), and width (mm), respectively.

2.4.2.2 Burst pressure and compliance

The theoretical burst pressure and compliance were approximated from the hoop stress vs strain curve using the thick-walled cylinder theory, *r / t < 10*. A simplified version of Lame's equations was used, which assumes negligible external pressure, negligible radial and axial stresses and strains, and maximum hoop stress at D_i (Equation 4).

$$\sigma_{hoop} = P_i \cdot \frac{r_o^2 + r_i^2}{r_o^2 + r_i^2} \quad \textbf{(4)}$$

Where P_i, r_o^2, and r_i^2 are the internal pressure (MPa), outside radius (mm), and inside radius (mm), respectively. The UTS_{hoop} was then used to determine the maximum P_i at failure which was then converted to mmHg (burst pressure).

The compliance was approximated by modifying Equation 5 to replace the diameter with strain as an input, as described below.

$$C_d = \frac{D_s - D_d}{(P_s - P_d)(D_d)} \; x\; 10^4 \quad [\%/\ 100\ mmHg] \quad \textbf{(5)}$$

Using the definition of strain, the circumferential length is converted to an equivalent diameter (Equation 6) and substituted into Equation 5, to yield Equation 7.

$$D_x = D_0\,(\epsilon_x + 1) \qquad [mm] \qquad \textbf{(6)}$$

$$C_d = \frac{\epsilon_s - \epsilon_d}{(P_s - P_d)(\varepsilon_d + 1)}\, x\, 10^4 \qquad [\%/\ 100\ mmHg] \qquad \textbf{(7)}$$

With the descriptions of the abbreviations used for Equation 5, Equation 6, and Equation 7 listed in **Table 2-4**.

Table 2-4: Descriptions and units of abbreviations for Equation 5, Equation 6, and Equation 7.

Abbreviation	Description and unit
C_d	Diametral compliance (%/ 100 mmHg)
D_s	Systolic diameter (mm)
D_d	Diastolic diameter (mm)
P_s	Systolic Pressure (MPa)
P_d	Diastolic Pressure (MPa)
D_x	Equivalent diameter at given strain (mm)
ε_x	Strain at the equivalent diameter
ε_s	Systolic strain at systolic hoop stress
ε_d	Diastolic strain at diastolic hoop stress

The equivalent diastolic and systolic hoop stress,σ_d and σ_s, were then determined at internal pressures of 80 mmHg (P_d = 1.07 x 10^{-2} MPa) and 120 mmHg (P_s = 1.6 x 10^{-2} MPa), respectively, using Equation 4. The corresponding strains were then read off from the stress-strain curves generated in section 2.4.2.1 UTS – Hoop stress, as illustrated in Figure 2-11. The strain values were then substituted into Equation 7 to determine the diametral compliance for each sample tested.

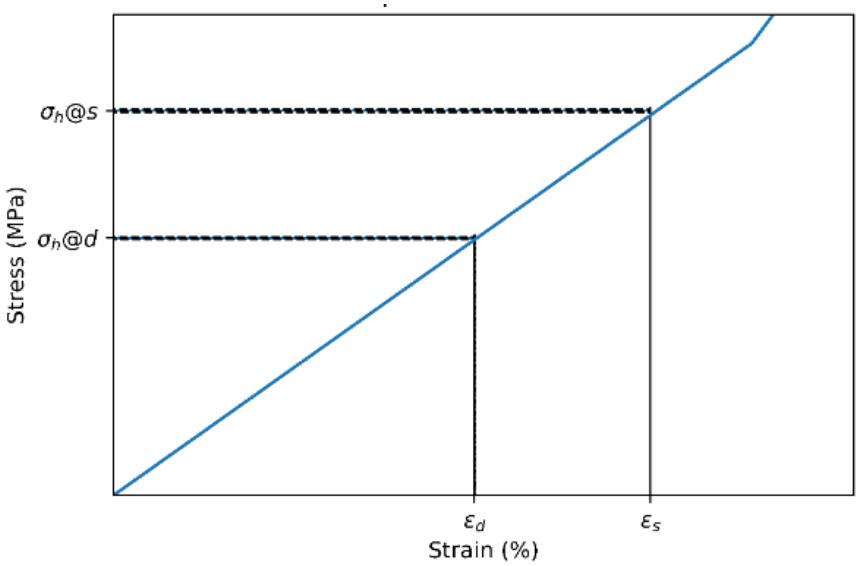

Figure 2-11: *Illustration of compliance calculations to obtain the equivalent systolic and diastolic strains*

2.5 Heparin incorporation

2.5.1 Heparin modification

Heparin ($HepNa^+$, porcine-derived, 12 kDa, 196 U/mg) was modified to heparin tributylamine (hepTBA) by ion-exchange to make it soluble in organic solvents to be used in electrospinning, as shown Figure 2-12 (76).

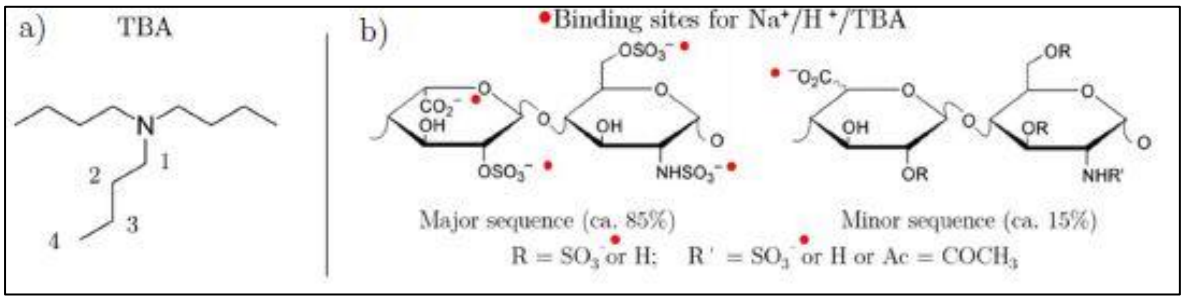

Figure 2-12: *a) Numbering reference of the methyl groups of tributylamine for NMR. b) Ion-exchange sites (red dots) for heparin molecule.*

1 g of $HepNa^+$ was dissolved in 100 mL of DI water (pH = 6.5). The Na^+ was exchanged with H^+ by passing the solution through a glass column (ID = 10.8 mm) packed with 7.5 g Dowex® resin (50Wx8[H^+], 200-400 mesh, Sigma Aldrich) at a flow rate of 5 mL/min (assisted with compressed air). Another 100 mL of DI water was passed through the resin bed to yield a 200 mL stock solution of heparin acid ($HepH^+$/DI water, 5 mg/mL, pH = 2.0).

HepTBA was produced by reacting 10 mL of a TBA/methanol solution (80mg TBA/ mL MeOH) with 40 mL of the $HepH^+$ stock solution (2 hours, stirred). The MeOH was evaporated (RII Rotavapor Buchi, 122 mbar, 40°C, 1 hour) until a volume of 40 mL remained and the unreacted TBA removed by liquid-liquid extraction (hexane, 3x100 mL). The HepTBA/DI solution was lyophilised (48 hours) to obtain a white, powdery product.

The degree of TBA complexation for the HepTBA was determined by the relative peak intensities between the methyl protons of TBA and the acetyl protons of heparin by ^1H NMR spectra in D_2O, described in section 2.5.2 Nuclear magnetic resonance spectroscopy. The complexation was quantified as a ratio between the integrated proton signals (**λ**) as described in Equation 8, with the functional groups of TBA correlating to that shown in Figure 2-12a.

$$\left(\frac{TBA_{methyl}}{Heparin_{acetyl}}\right)_{^1H\ NMR} = \frac{1}{4}.\frac{\left(\frac{\int_H \lambda_{TBA_1}}{2} + \frac{\int_H \lambda_{TBA_2}}{2} + \frac{\int_H \lambda_{TBA_3}}{2} + \frac{\int_H \lambda_{TBA_4}}{3}\right)}{\frac{\int_H \lambda_{Heparin}}{3}} \quad \textbf{(8)}$$

2.5.2 Nuclear magnetic resonance spectroscopy

The compounds were prepared by dissolution (4 mg/mL) and microfiltration (0.45 µm) in heavy water (D_2O). The Nuclear Magnetic Resonance (NMR) spectra were recorded at RT using a spectrometer (Bruker DRX-400, 10 s recycle delay. 128 scans). The signals were processed for phase correction, baseline subtraction, and numerical integration (MestReNova, v 11.0, Spain).

2.5.3 *In vitro* heparin release

The HepTBA electrospun vascular grafts (1 mm in length) were immersed in 1 mL of PBS in sealed plastic tubes and incubated at static conditions (37°C). The elution fluid was collected and replaced with new PBS at set time points (**Table 2-5**).

Table 2-5: Drug elution time points for *in vitro* studies.

Sample	Time points (days)	Sample size (n)
DP30	1, 2, 3, 4, 5, 6, 14, 21, 28	3
DP30 + 3% HepTBA	1, 2, 3, 4, 5, 6, 14, 21, 28	3
DP30 + 5% HepTBA	1, 2, 3, 4, 5, 6, 14, 21, 28	3

The eluates were analysed for their heparin content using a modified 3-methyl-2-benzothiazolinone hydrazone hydrochloride (MBTH)-assay. Each eluate (250 µL) was sonicated (30min, RT) with 500 µL nitrous acid solution (0.025 M HNO_2, 1 M HCl) prior to the addition of 250 µL ammonium sulfamate solution (1 M). The mixture was diluted with 300 µL NaCl solution (1 M) and sonicated (15min, 50°C) with 500 µL MBTH solution (0.011 M) followed by the addition of 500 µL of $FeCl_3$ solution (0.031 M) and sonicated for another 20 min (50°C).

The colourimetric solutions were then transferred to disposable cuvettes to measure their absorbances with UV spectroscopy (wavelength: 660 nm). A standard absorbance curve was generated, at known concentrations of HepTBA, to calculate the concentration (mg/mL) of released HepTBA for each eluate. Instantaneous and cumulative delivery rates were expressed as mg HepTBA/g scaffold.

2.6 Degradation study

The degradation study was conducted to determine the *in vitro* strength loss over time. The grafts were tested as described in section 2.4.1 Longitudinal tensile testing and 2.4.2 Circumferential tensile testing.

The samples were sealed in tubes and incubated at static conditions in PBS (37°C). The samples (gauge length: 10mm, n = 3) tested in the longitudinal direction were incubated in

2 mL of PBS, whereas the samples (width: 5mm, n = 3) tested in the circumferential direction were incubated in 1 mL of PBS. The groups tested with their time points are listed in **Table 2-6**.

Table 2-6: Time points and sample size for groups tested for mechanical strength loss *in vitro*.

Sample	Time points (days)	Sample size (n)
DP30	7, 14, 28	3
DP30 + 3% HepTBA	7, 14, 28	3

2.7 *In* vivo performance

The *in vivo* performance of the electrospun biodegradable vascular grafts developed during this project was investigated using a rat infrarenal aortic model (as previously used by UCT Cardiovascular Research Unit (89, 119, 120) and others specific for electrospun vascular grafts (24, 80, 97, 104). Note that this was a pilot implant to test the feasibility and get the first indication of tissue ingrowth only and not a full study with full histological analysis, as the latter falls outside the scope of this study.

All procedures were in accordance with the Animal Protection Act (Act 70 of 1962), the Veterinary and Para-veterinary Professions Act (Act 19 of 1982) and the South African National Standard for the Care and Use of Animals for Scientific Purpose (SANS 10386:2008). This study (protocol no. 018 – 038) was approved by the Departmental Research Committee and the Animal Ethics Committee of UCT. The individuals involved in the handling of the animals were all trained and registered as veterinarians or para-veterinarians with the South African Veterinary Council (SAVC). The registration number for the author of this thesis: AR18/16768.

The following sections provide i) an overview of the study, ii) parameters for manufacturing of the vascular grafts, iii) the implant end explant procedure, and iv) the histological analysis.

2.7.1 Graft manufacturing for implantation and study overview

The vascular grafts chosen for the *in vivo* evaluation are DP30 and DP30+3%HepTBA. The parameters to manufacture these grafts can be viewed in Table 2-2. Figure 2-13 is an overview of the pilot study. The 6 animals were issued 3 days in advance for acclimatisation and handling. They were hydrated and fed *ad libitum*.

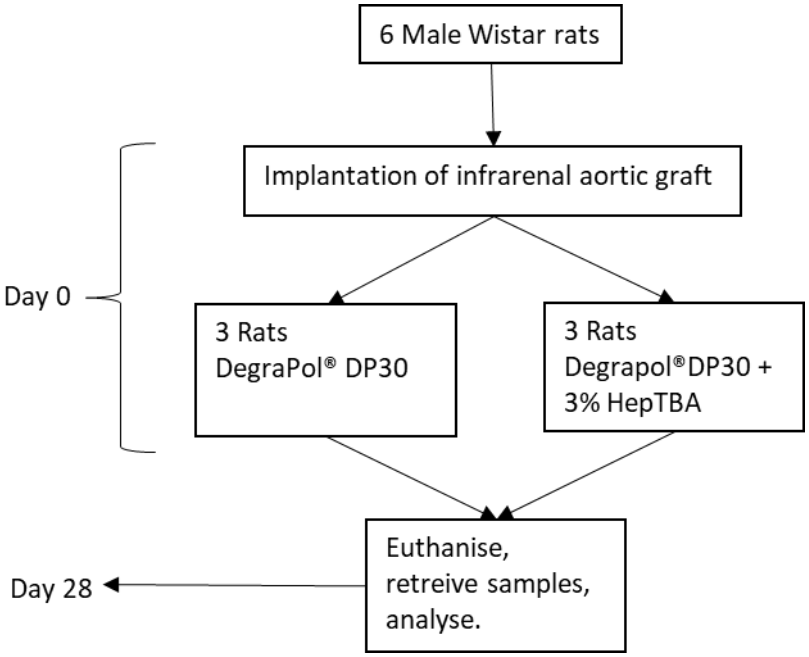

Figure 2-13: *Circulatory model design overview.*

2.7.2 Graft implant and explant procedure

2.7.2.1 Preoperative preparation

The animal was weighed and anaesthetised, in an induction chamber, using isoflurane (5%, oxygen flow rate 2 L/min) for approximately 3 minutes, or until the rat has lost consciousness and the breathing was observed to be regular.

The incision site was prepared by carefully shaving the abdomen and sterilising the skin with F10® solution and iodine. Volatile anaesthesia was maintained at 1.5 - 2% of isoflurane at an oxygen flow rate of 2 L/min. Buprenorphine (0.05 mg/kg) was administered (SC), ocular lubrication was applied to prevent corneal desiccation.

2.7.2.2 Surgical procedure

A laparotomy was performed via a ventral midline incision from the pubis to the xiphoid process using aseptic techniques. The gastrointestinal tract was then lifted and placed outside the abdominal cavity, on sterile drapes. The infrarenal abdominal aorta was identified and dissected to expose the renal arteries to the iliac bifurcation. The aortic branches were cauterised and the infrarenal aorta fully mobilised. Heparin solution (1 mg/kg) was administered in the iliolumbar vein as part of the standard procedure for vascular anastomosis. The graft was then cut to the required length (± 1.8 cm).

The vessel was clamped proximal and distal to the site of the graft, the infrarenal aorta was then divided without excising it. The exposed lumens were washed with heparin solution (1 mg/kg) to dissolve any clots and the graft anastomosed proximally and distally with 8-12 interrupted 9 - 0 nylon sutures (Ethilon; Johnson & Johnson, New Brunswick, NJ). On completion of anastomoses, the distal clamp was released first to fill the graft with blood, while the proximal clamp was replaced with a hand-controlled clamp. Direct compression to the anastomotic sites was applied to obtain haemostasis. The graft was monitored for an additional 5 minutes to ensure that there is no haemorrhage.

The isoflurane was decreased to 0.5% and a visual patency test was performed prior to closing the abdominal cavity in two layers using a non-absorbable coated braided suture. (2-0 Ethibond, Johnson & Johnson, New Brunswick, NJ). The abdominal sheath was closed in a continuous manner form the subxiphoid process to the suprapubic region. The closure of the skin was performed in a continuous manner. Buprenorphine (0.05 mg/kg) was administered twice daily for three consecutive days as analgesia.

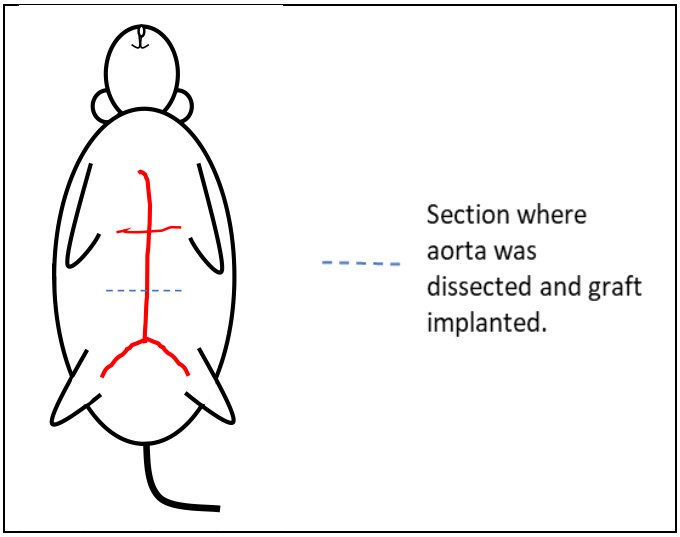

Figure 2-14: *Illustration of surgical procedure for the circulatory model.*

2.7.2.3 Ultrasonography procedure

Ultrasound evaluation of the graft was conducted on day 7,14,21 and 28. The animals were premedicated with buprenorphine (0.05 mg/kg), 30-45 minutes before the procedure as a sedative and for pre-emptive pain management. The animal was anaesthetised, the hair was removed from the abdominal area with dilapidating cream (Nair®, Hair removal cream, US, Figure 2-15A). Doppler ultrasound was conducted to determine the patency of the aorta/graft with various Doppler ultrasonography modalities (Figure 2-15B).

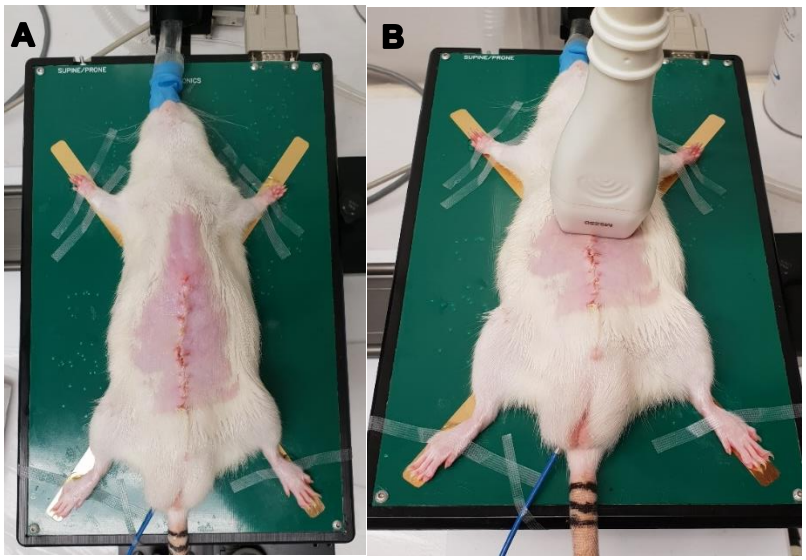

Figure 2-15: *Ultrasonography procedure. A) Preparation B) Ultrasonography conducted*

2.7.2.4 Explant procedure

Each explant occurred at 28 days after implantation. The animal was anaesthetised and the abdomen was re-entered via the same incision site. The infrarenal graft was identified and surrounding adhesions dissected and freed. The distal aorta was checked for patency before intravenous injection of heparin (1 mg/kg) was administered via the inferior vena cava. After 3 minutes has passed the animal was euthanised by exsanguination via an incision into the right atrium of the heart. A 30G cannula was advanced into the ascending aorta via the apex of the left ventricle and angiography performed with a single dose of 5 mL iodine contrast. The images were acquired with the use of a C-arm (Phillips® BV Pulsera, Massachusetts, US).

The aorta was flushed with a heparinised normal saline (5000 IU/1 L) via the left ventricle. The graph was sectioned and fixated in a zinc salt solution for histology.

2.7.3 Histology

2.7.3.1 Fixation and staining

The grafts explanted were divided with a 5 mm mid-graft cross-sectioned, with the remaining proximal and distal segments cut longitudinally and fixed in a zinc salt solution for histology (Figure 2-16).

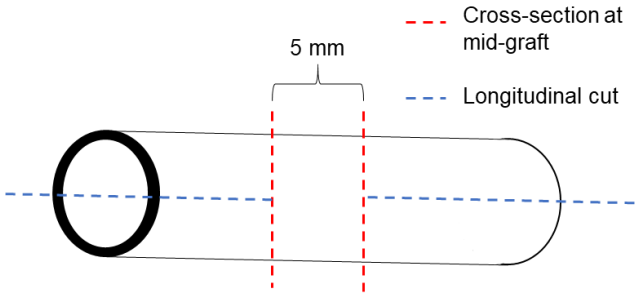

Figure 2-16: *Graft section to be fixed in a zinc salt solution for histology.*

The fixed samples were stained with haematoxylin and eosin (H&E, Merck, Germany, and BDH, England) and Miller and Masson elastin trichrome (Elmas, Fitzgerald International, MA) for immunohistochemistry to label cell ingrowth.

The slides were photographed with a Nikon Eclipse 90i stereo microscope (with a fluorescence unit, Nikon, Japan) equipped with a digital camera (DS-Ri1, Nikon, Japan). H&E stains were captured using 2X and 10X magnification, whereas the Elmas stain was only captured with a 2X magnification (1.0X digital zoom, 3.22 µm/pixel calibration and analogue gain of 1.0X), These micrographs were only used as a feasibility study, therefore no quantification of tissue ingrowth, endothelialisation or vascularisation was done.

2.8 Statistical analysis

All data were expressed as mean±standard deviation, except the fibre diameter for the parametric study was expressed as mean±standard error of the mean. The data sets were analysed for their variance and significance (P value) using a one-way ANOVA and a two-tailed, equal variance t-test if found significant. $P<0.05$ was assumed to be significant between the data sets. The plotting of the graphs and computations were done with Python (Spyder, Version 3.3.2).

3 Results and Discussion

This chapter presents the results obtained under four main headings, namely; Electrospinning humidity control unit, Parametric study, Drug incorporation and elution, and Vascular grafts in *vivo* implantation – Pilot study. The subsections will include the efficacy of the electrospinning rig design, thereafter the results of the morphological and mechanical properties of the grafts produced in the parametric study, drug incorporation and HepTBA elution results. Finally, the *in vivo* evaluation of the grafts produced for the pilot study.

3.1 Electrospinning humidity control unit

The ambient rH was measured as 59% rH (23°C, red line) at time point 0 (Figure 3-1). The drying loop took approximately 18 min to reach the set point ABC, 19 min to reach set point DEF and 15 min to reach set point GH. The rH was maintained from B to C and E to F, with minor fluctuations (±2% rH). Figure 3-1 illustrates the efficacy of the unit to adjust the rH, above and below the ambient rH, and reach it multiple times which indicates that control was maintained over the rH.

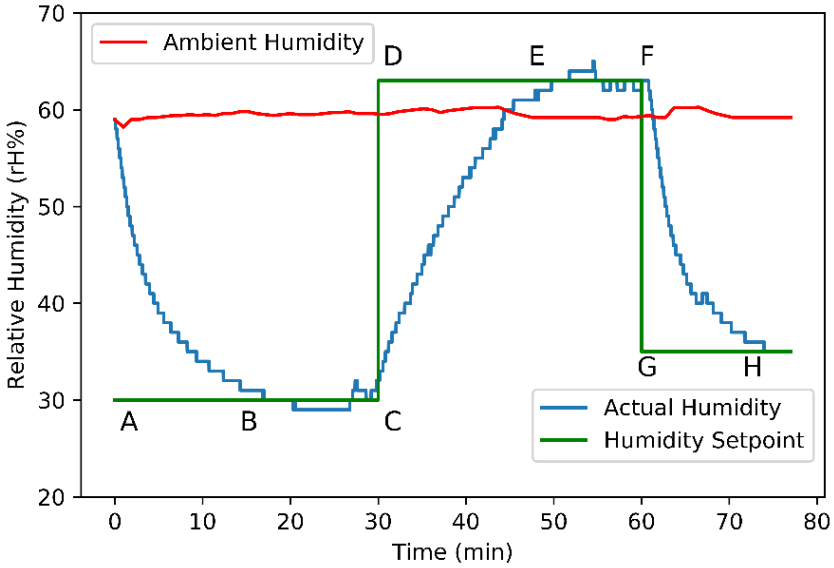

Figure 3-1: *Efficacy of the drying and wetting of the electrospinning humidity control unit (T = 23°C).*

3.2 Parametric study

The influence of the solvent system and humidity (input parameters) on the fibre morphology and mechanical properties was quantified for the electrospun vascular grafts. The results are discussed in the following sub-sections.

3.2.1 Fibre morphology

The fibre diameter (Figure 3-2A) coherency (orientation index, OI, Figure 3-2B), pore size (Figure 3-3) and porosity (Figure 3-4) quantified are presented and discussed in this section.

3.2.1.1 Fibre diameter

The mean fibre diameter between all the groups electrospun from $CHCl_3$, 1% HFIP, 5% HFIP at a rH of 30%, 40%, and 50% was 4.12±0.92µm. Irrespective of the solvent system used, there was no statistically significant effect of rH on fibre diameter. The effect of rH on fibre diameter has been shown to be variable and depend on the polymer and solvents used (62).

The addition of HFIP seem to result in decreased fibre diameters at 30% rH and 50% rH, but the effect is not statistically significant. However, when scaffolds from the pure chloroform group were visually compared to those from the 5% HFIP solution, the fibre diameters decreased, as well as a film formation on the lumen (Figure 3-5). Reduced fibre diameters were expected with higher concentrations of HFIP, due to a higher dielectric constant inducing a longer jet stretching and whipping region (121).

It was also noticed that the lumen had thicker fibres than the ablumen (**Figure 3-5**) for the solvent groups used, with the largest fibre diameters obtained from the pure chloroform solvent system, which indicates 'wet landing' of the fibres. The effect dissipates at the ablumen, showing cylindrical fibres, as the wall thickness of the graft increase, therefore altering the electric field acting on the fibres from the mandrel.

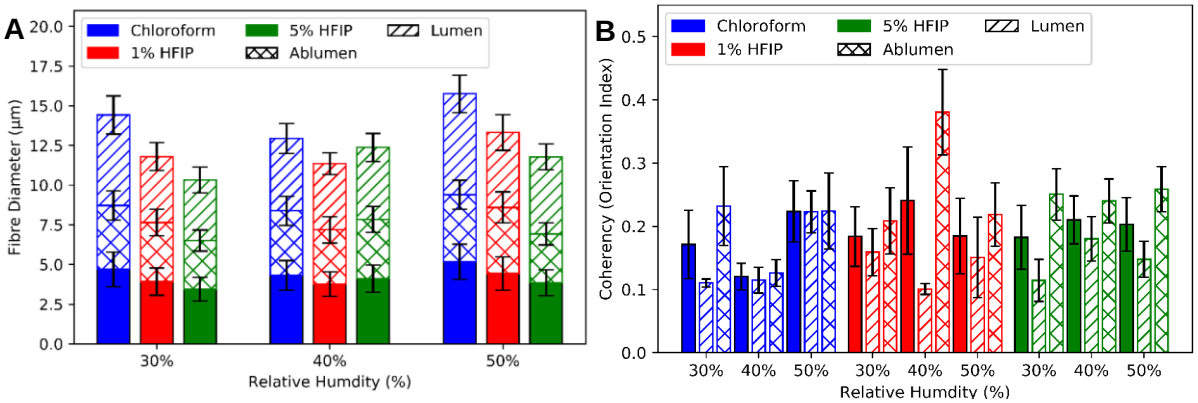

***Figure 3-2**: Fibre diameter and coherency of the DP30 electrospun vascular grafts with pure chloroform, 1% HFIP, and 5% HFIP as the solvent at 30%, 40%, and 50% relative humidity. A) Fibre diameters of the lumen, ablumen, and the average between the lumen and ablumen (solid fill). B) Orientation Index of the lumen, ablumen, and the average between the lumen and ablumen (solid fill).*

3.2.1.2 Fibre coherency

The mean OI between the solvent groups and the rH range were 0.19±0.11. The effect of rH and solvent system on the OI was not statistically different, except for the lumen and ablumen with the 1% HFIP group at 40% rH ($P<0.05$). However, the ablumen (1%HFIP, 40% rH) data point is an outlier and cannot be compared to the lumen of the same group. A solvent system with a higher dielectric constant should produce more randomly oriented fibres, which was not the case with the addition HFIP compared to pure chloroform. It is expected that pure chloroform as the solvent should produce more aligned fibres, in the circumferential direction. This phenomenon may have been negated by the slow rotation speed (150 RPM) and small diameter mandrel, giving similar OI for the solvent systems.

3.2.1.3 Pore size

The mean equivalent pore diameter for the $CHCl_3$, 1% HFIP, and 5% HFIP groups were 8.0±8.6 µm, 7.9±7.4 µm, and 5.9±5.7 µm, respectively with a maximum mean pore size of 10.9±9.6 µm (Pure chloroform, 30% rH). Although increasing rH had a statistically significant effect on the mean equivalent pore diameters for the respective $CHCl_3$ and 5% HFIP groups, no trend could be observed (Figure **3-3**). It is well described that an increase in pore size can be obtained with an increase in fibre diameter (122-124), the change in pore size of the scaffolds over the rH range cannot be attributed to the increase in fibre diameter, as this was statistically insignificant, as previously discussed. The statistical difference between the groups is a result of large data sets.

The mean pore size of the 0%, 1%, and 5% HFIP solution was 10.9±9.6 µm, 8.2±6.8 µm, and 4.9±4.8µm ($P<0.0001$) respectively, at 30% rH which clearly indicates a decrease in pore size with an increase in HFIP concentration. The same trend was observed at 40% and 50% rH, although the $CHCl_3$ solution had a smaller mean pore size (5.9±7.3 µm) than the higher concentrations of HFIP(8.3±8.0 µm and 6.85±6.75 µm for 1% and 5% HFIP respectively). This lines up with the effects of fibre diameter on pore size, with a solution of higher conductivity resulting in smaller fibre diameters and smaller pore sizes, as can be seen with an increase in HFIP concentration. However, observable film formation due to wet landing and fibre fusion with increasing HFIP concentration contribute to the decrease in mean pore size. This effect is observed at increasing rH as well (Figure 3-5).

3.2.1.4 Porosity

The mean porosity ranged between 35%-65% between the input parameters, with maximum porosities obtained at 30% rH for all the solvent systems (44.2±7.0%, 60.6±2.1%, 54.0±3.6% for the $CHCl_3$, 1% HFIP, and 5% HFIP groups respectively).

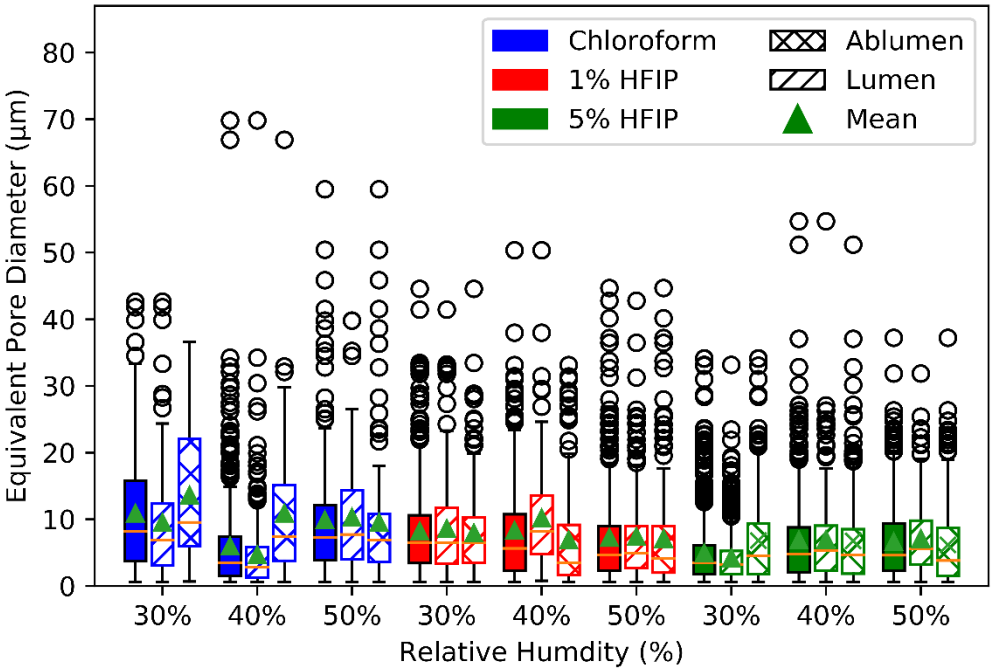

Figure 3-3: *Box and whisker plot of the equivalent pore diameters the DP30 electrospun vascular grafts with pure chloroform, 1% HFIP, and 5% HFIP as the solvent at 30%, 40%, and 50% relative humidity., illustrating the outliers (circles), median (orange line), and mean (green triangle) of the lumen, ablumen, and average between the lumen and ablumen (solid fill).*

A monotonic decrease was only observed for the 1% HFIP solvent system ($P<0.01$) throughout the rH range, whereas the $CHCl_3$ and 5% HFIP solutions had an increase in porosity from 40% to 50%. However, the increase in porosity from 40% rH to 50% rH for the $CHCl_3$ and 5% HFIP solutions was not statistically different. Therefore, it seems that increasing rH decrease the porosity for all the solvent groups. The decrease in porosity with an increase in rH is due to more fibre fusion and film formation.

Addition of HFIP increased the porosity of the scaffold over the rH range, however, a decrease in porosity was obtained when the 5% HFIP group was compared to the 1%HFIP group. The addition of HFIP was expected to decrease the porosity of the grafts however, it only started to decrease at higher concentrations of HFIP (5%). To add to this mystery chloroform also had the largest pore sizes, therefore a decrease in pore size compared to 1% HFIP is unexpected. If the SEM images are visually compared (Figure 3-5), the lumen of the pure chloroform DP30 grafts had thicker fibres and more fusion, compared to higher concentrations of HFIP however, this was not the case with the ablumen. It may be that the pores weren't interconnected which may influence the values of the hydrostatic weighing upon porosity calculations.

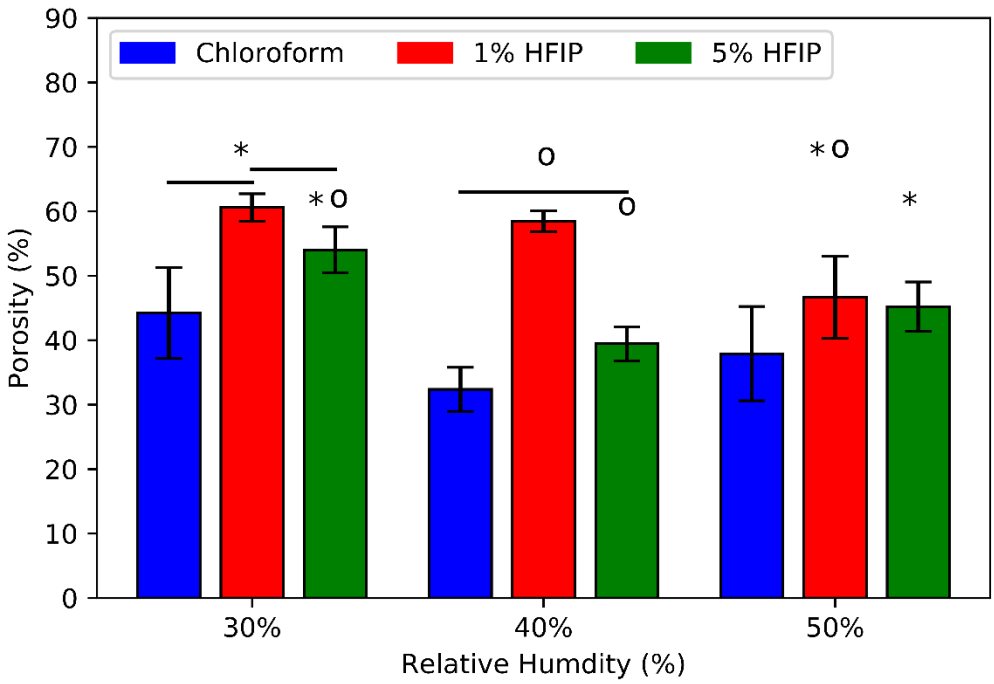

Figure 3-4: *Porosity of the DP30 electrospun vascular grafts with pure chloroform, 1% HFIP, and 5% HFIP as the solvent at 30%, 40%, and 50% relative humidity. Solid bars indicate statistical significance between the solvent systems at a specific rH, '*' and 'o' indicate statistical significance between the different rH for a specific solvent.*

It is still a confounding factor as to how previous researchers achieved such high porosities (>70%) with pure chloroform as the solvent (33, 83, 114, 116, 125, 126) with only a few using a mixture of chloroform and HFIP(81, 82, 127), however it is clear that at higher concentrations of HFIP the degree of fibre fusion and film formation will increase.

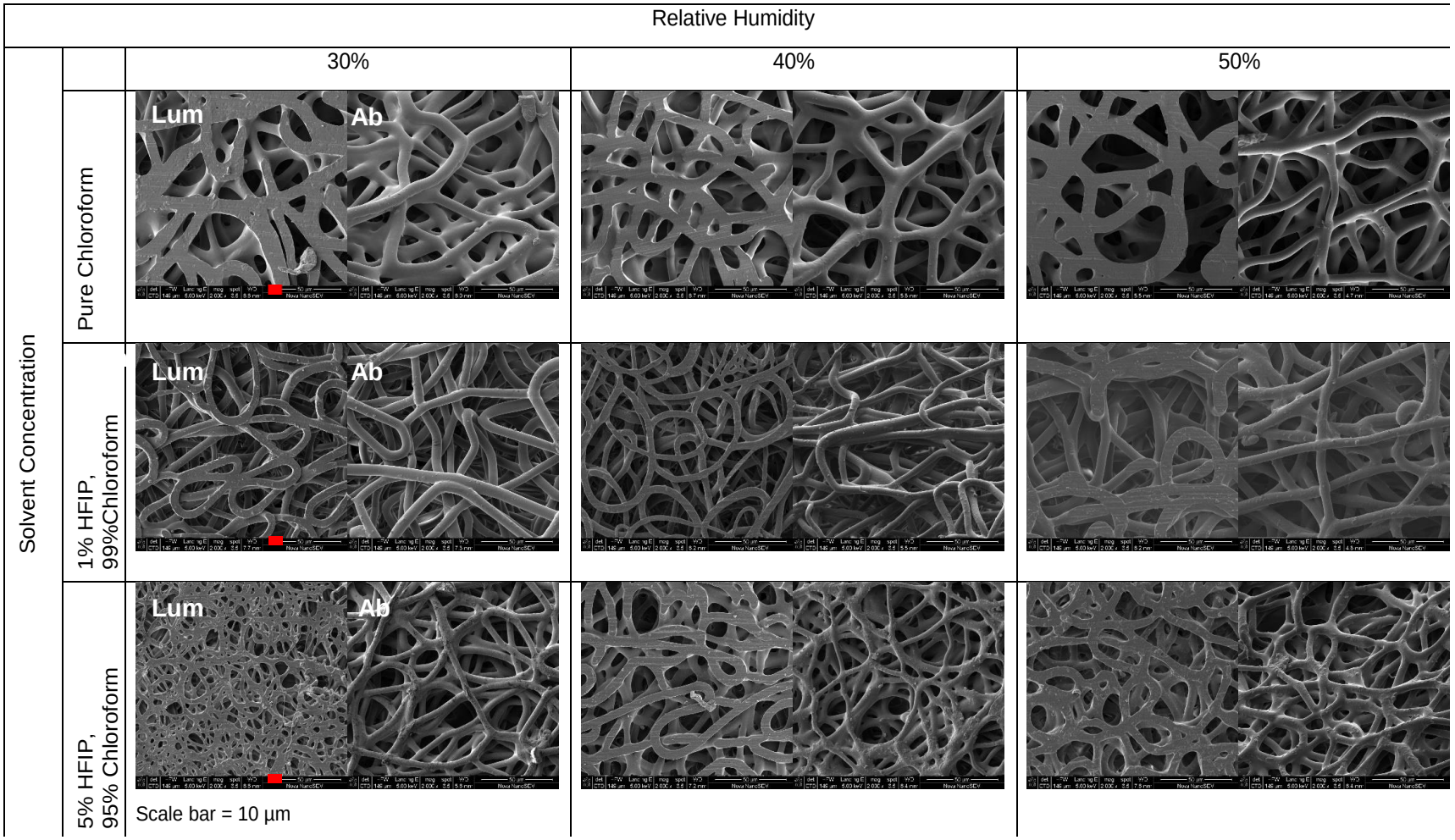

Figure 3-5: *SEM images of the DP30 electrospun vascular grafts with pure chloroform, 1% HFIP, and 5% HFIP as the solvent at 30%, 40%, and 50% relative humidity. Lum = Lumen (Left), Ab = Ablumen (Right). Scale bar = 10 µm*

3.2.2 Mechanical properties

3.2.2.1 Circumferential mechanical properties

The circumferential ultimate tensile strength (UTS), maximum strain (ε_{max}), and Young's Modulus (E_Y) of the three solvent systems, at a rH of 30%, 40%, and 50%, are shown in Figure 3-6.

An increase in rH had a small but insignificant increase on the UTS (hoop stress) and maximum elongation of the solvent groups (Figure 3-6A and Figure 3-6B). However, when the solvent groups were compared to each other, the UTS of the $CHCl_3$ group was on average 2.9±0.6 times higher than solutions containing HFIP ($P<0.05$), with an average of 0.63±0.16 MPa for the chloroform solvent system. Similarly, the mean maximum elongation for the $CHCl_3$ solvent system was 90±16% versus 39±9% for the HFIP groups.

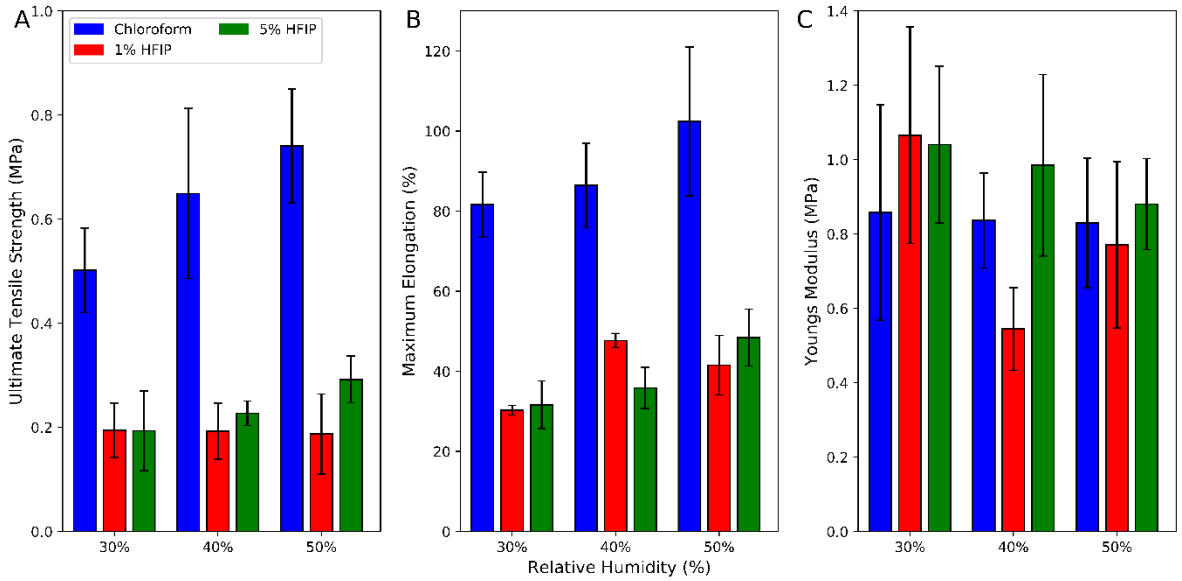

Figure 3-6: *Circumferential mechanical properties of the DP30 electrospun vascular grafts with pure chloroform, 1% HFIP, and 5% HFIP as the solvent at 30%, 40%, and 50% relative humidity. A) Ultimate tensile strength (UTS). B) Maximum strain (elongation). C) Young's Modulus.*

The input parameters had an insignificant effect on Young's Modulus (Figure 3-6C) and the compliance (Figure 3-7A) of the scaffold, therefore an average E_Y was calculated for each of the three different solvent systems over the rH range of 0.84±0.21 MPa, 0.82±0.31 MPa, and 0.97±0.21 MPa for pure chloroform, 1% HFIP, and 5% HFIP solvent systems, respectively. The average compliance between all the input parameters was 8.4±1.7%/100mmHg.

The burst pressure was approximated from the UTS, therefore it was influenced in the same way by the input parameters as the UTS. $CHCl_3$ had an average burst pressure of 910±134 mmHg versus 320±84 mmHg for the HFIP solvent systems (P<0.05).

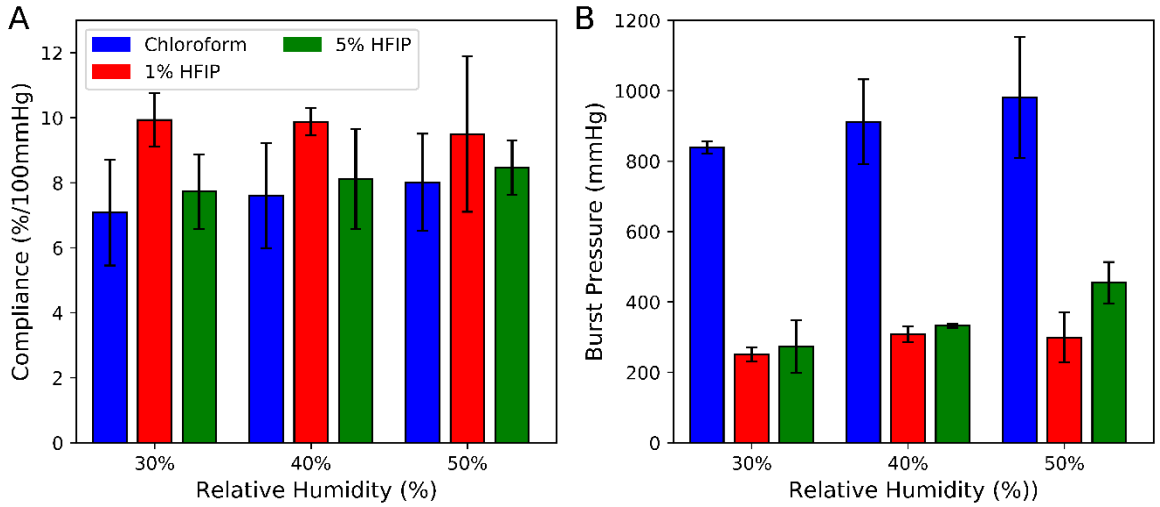

Figure 3-7: *Compliance (A) and burst pressure (B) of the DP30 electrospun vascular grafts with pure chloroform, 1% HFIP, and 5% HFIP as the solvent at 30%, 40%, and 50% relative humidity.*

The effect of increasing UTS and strain of the scaffolds spun from pure chloroform compared to those containing HFIP are due to the decrease in porosity as described by Milleret, Simona (116), although it had no statistically significant effect on Young's Modulus and compliance. The compliance is still within the physiological range of 6-12%/ 100mmHg as defined by Tai, Giudiceandrea (128) in a healthy patient's common femoral and popliteal arteries. The burst pressures of the different solvent systems are higher than the average blood pressure of a healthy person (120 mmHg/70 mmHg), with the pure chloroform solvent system at approximately 6 times more. The increased burst pressure for this solvent system is due to the decrease in porosity, as the burst pressure is approximated from the UTS, therefore a change in the UTS will have a proportional change to the burst pressure.

3.2.2.2 Longitudinal mechanical properties

Although insignificant, an increase in longitudinal UTS with higher rH was observed with a mean UTS's of 1.1±0.7 MPa, 0.8±0.5 MPa, and 1.5±0.3 MPa for pure chloroform, 1% HFIP, and 5% HFIP respectively (Figure 3-8A). Initially, the addition of HFIP decreased the UTS however, when the 5% HFIP solution was used an increase was seen when compared to the $CHCl_3$ group.

The same trend was noticed for the maximum strain (Figure 3-8B), with no statistical significance between the different rH for the solvent systems, with a mean ε_{max} of 21.6±7.5%,

24.9±10.1%, and 34.1±9.8% for pure chloroform, 1% HFIP, and 5% HFIP respectively. The addition of HFIP had a 1.5-fold increase in the strain at 30% rH ($P<0.05$), whereas at 40% rH the 5% HFIP group had a 2.2-fold increase in maximum strain ($P<0.05$), compared to the pure chloroform group.

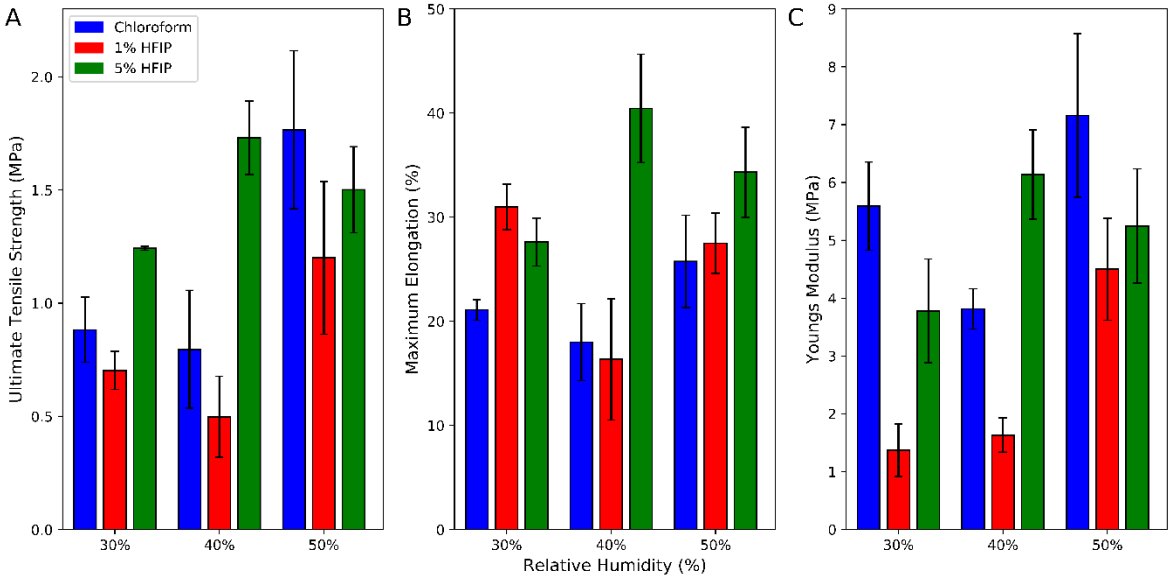

Figure 3-8: *Longitudinal mechanical properties of the DP30 electrospun vascular grafts with pure chloroform, 1% HFIP, and 5% HFIP as the solvent at 30%, 40%, and 50% relative humidity. A) Ultimate tensile strength (UTS). B) Maximum strain (elongation). C) Young's Modulus.*

The mechanical properties in the longitudinal direction did not follow the same trend as for the circumferential direction. The UTS and strain were similar between the solvent a rH groups with a slight increase in stress and strain with increasing HFIP concentration and rH. The UTS values for the pure chloroform system are similar in the longitudinal and circumferential direction, which confirms randomly orientated fibres. However, the same effect is not seen with the decrease in strain. The higher concentrations of HFIP have increased UTS's and may be as a result of more aligned fibres in the longitudinal direction. This is due to a combination of increased conductivity of the solution, small diameter mandrel, and low rotating speed. The slow rotation makes it difficult to align fibres circumferentially, with the whipping of the high conductive solution results in fibre deposition along the axial direction.

3.3 Further development of electrospun vascular graft

An acute animal study was approved to test the handling, strength and size of the electrospun vascular grafts in a rat (350 g – 450 g) infrarenal aortic implantation model. The electrospun vascular graft chosen after the tests from the parametric study was DP30 with pure chloroform

as the solvent at 30% rH, due to its superior pore size and mechanical properties. The mechanical and morphological properties of the chosen graft are listed in **Table 3-1** and **Table 3-2**.

Table 3-1: Mechanical properties of the electrospun DP30 vascular graft for the acute in vivo study.

Property	Results
UTS	0.50±0.08 MPa – C*, 0.9±0.5 MPa – L*
Maximum Strain	81.7±8.0% - C, 21.1±2.0% - L
Young's Modulus	0.9±0.3 MPa – C, 5.9±1.5 MPa – L
Compliance	7.1±1.6%/100mmHg
Burst Pressure	839±17 mmHg

*C = Circumferential. L = Longitudinal.

Table 3-2: Morphological properties of the electrospun DP30 vascular graft for the acute in vivo study.

Property	Results
Fibre diameter	3.9±1.0 µm
Fibre coherency (OI)	0.17±0.05
Equivalent pore diameter	10.9±9.6 µm
Porosity	44.2±7.0%
Length	1.8±0.2 mm
Wall thickness	400±100 µm
Inner diameter	2.1 mm

In the acute in vivo study, it was noticed that the 2.1 mm (ID) electrospun vascular graft was oversized when compared to the infrarenal aortic diameter of the rats available at the time (Figure 3-9). This resulted in further development of the electrospun graft by decreasing the mandrel OD to 1.7 mm.

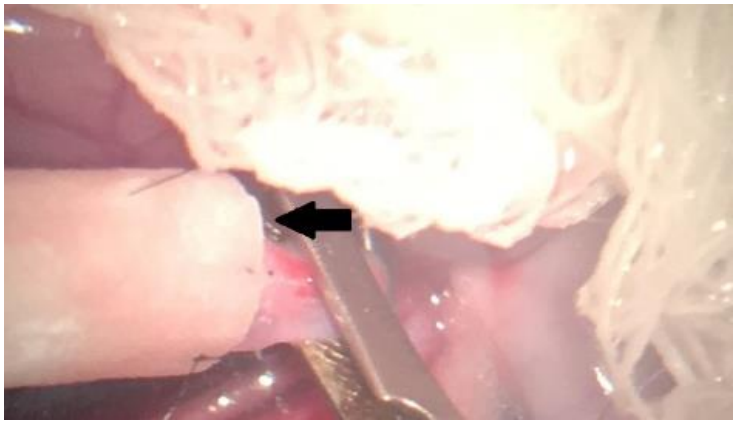

Figure 3-9: *Acute in vivo study of DP30 electrospun vascular graft in a rat infrarenal aortic model comparison. Arrow indicates the discrepancy between the outer diameter of the native aorta and inner diameter of the electrospun vascular graft.*

3.3.1 Drug incorporation and elution

The drug release profiles for the DP30 electrospun vascular grafts containing 3wt% and 5wt% HepTBA for a period of 28 days are shown in Figure 3-10.

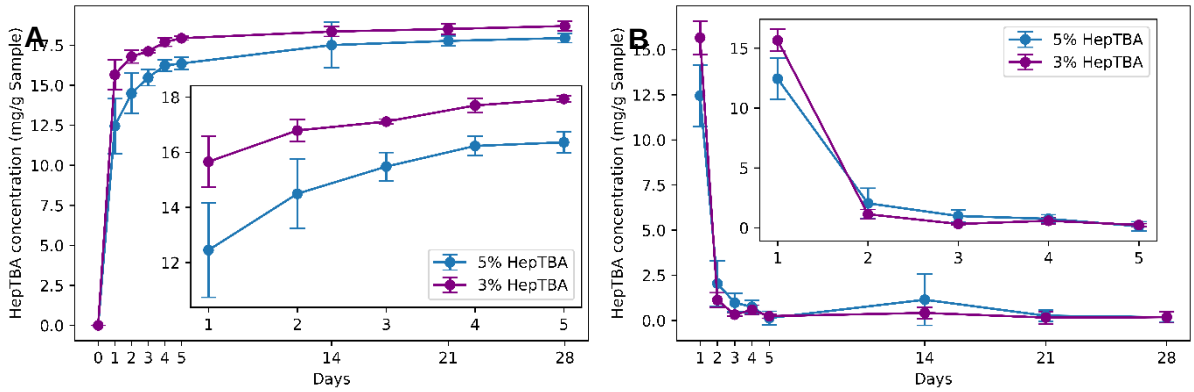

Figure 3-10: *HepTBA release curves for 5% and 3% HepTBA (w% HepTBA/w polymer). A) Cumulative release curve from day 0-28. B) Instantaneous release curve from day 1-28. *Insets: Enlarged release curves from day 1 to 5.*

Figure 3-10A shows a cumulative dosage of 25%, 33%, and 36% of the total HepTBA (50 mg/g DP30) was released on day 1, 5, and 28 respectively, for the 5% HepTBA graft. The 3% HepTBA graft had a faster release rate with 52%, 60%, and 62% of its load (30 mg/g DP30) being released on day 1, 5, and 28 days, respectively. The instantaneous release curve (Figure 3-10B) shows that there was a significant decrease in HepTBA being released between day 4 and 5 with 0.586 mg/g DP30 to 0.237 mg/g DP30 and 0.750 mg/g DP30 to 0.131 mg/g DP30, respectively for 3% ($P<0.05$) and 5% HepTBA ($P<0.05$).

The cumulative and instantaneous release curves (Figure 3-10A and Figure 3-10B) show that both concentrations of HepTBA had a burst release on day 1 with a significant amount of HepTBA still being released at day 4, whereafter it plateaus out. This is consistent with the study of Kwon and Matsuda (76) where he eluted 1%, 5%, and 10% HepTBA from PLCL electrospun scaffolds. Although it does not explain the larger amount of 3% HepTBA being released compared to 5%, which is counterintuitive. The only possible explanation is that the 5% HepTBA was not fully dissolved in the solution, although it was dissolved until a clear solution was obtained, therefore the actual amount of HepTBA incorporated was less than initially expected. It can also be seen that the amount of HepTBA converges to the same point at day 28, which strengthens the possibility that there may have only been about 3% HepTBA in the graft. This, however, cannot be fully confirmed unless the elution study was done until the graft was fully degraded. The authors of Kwon and Matsuda (76) as well as previous research done in this lab (unpublished data) did not achieve cumulative release of more than

53% for their total loads after 4 weeks, with 36% of the 5% HepTBA load being released, which is in line with the 36% release of 5% HepTBA from this study. It should be noted that a maximum of 10% HepTBA was used by Kwon and Matsuda (76), with HFIP as a solvent, which dissolves HepTBA more readily. The 3% HepTBA achieved a cumulative release of 62% after 28 days, which is far greater release than previously document in the literature as well as in this research group. It is assumed that the rest of the HepTBA is embedded within the graft.

The modification of $HepNa^+$ to HepTBA made it possible for heparin to be soluble in organic solvents, such as chloroform, however, the solubility was dependent on the degree of complexation of the tributylamine to $HepH^+$. This made the solubility of a DP30+5% HepTBA solution inconsistent. Excess reagent was used and therefore the degree of complexation cannot be the overall reason for the inconsistencies in solubility, with the $HepH^+$, being fully complexed. The limiting step is believed to be the ion exchange site from $HepNa^+$ to $HepH^+$ in the filtration bed with packed with Dowex®. The flow rate of the $HepNa^+$ solution was assisted with compressed air, with no fine control over the pressure of the compressed air, the solution may have passed through the packed bed to quickly, not allowing sufficient time for ion-exchange. Another plausible explanation is that the pressure may have collapsed the filtration bed, inducing a crack where the solution passes through and saturating that section of the bed, not allowing for complete ion exchange. The decrease in H^+ binding sites decreases the amount of TBA able to complex to the $HepH^+$, irrespective of the excess amount of TBA added. This decrease the solubility of the HepTBA in chloroform.

The burst release of the HepTBA, as well as the remaining embedded HepTBA, may be beneficial for an anti-thrombotic lumen and prevent SMC proliferation and intimal hyperplasia of the electrospun vascular graft (44, 129).

The DP30+3% HepTBA electrospun graft was chosen for further testing, due to its similar drug release profile to 5% HepTBA as well as its consistent solubility in chloroform.

3.3.2 Fibre morphology of *in vivo* grafts

The DP30 and DP30 + 3% HepTBA grafts were analysed for the fibre morphology and the results are presented in Figure 3-11.

Fibre diameter: The mean fibre diameters for the DP30 and DP30+3%HepTBA electrospun grafts (Figure 3-11A) were 5.97±1.57 µm and 3.45±1.69 µm ($P<0.01$), respectively. This is due to the increased solution conductivity with the addition of a salt (HepTBA), increasing the

length of the straight jet portion as well as stretching of the whipping radius, producing thinner fibres(58, 60).

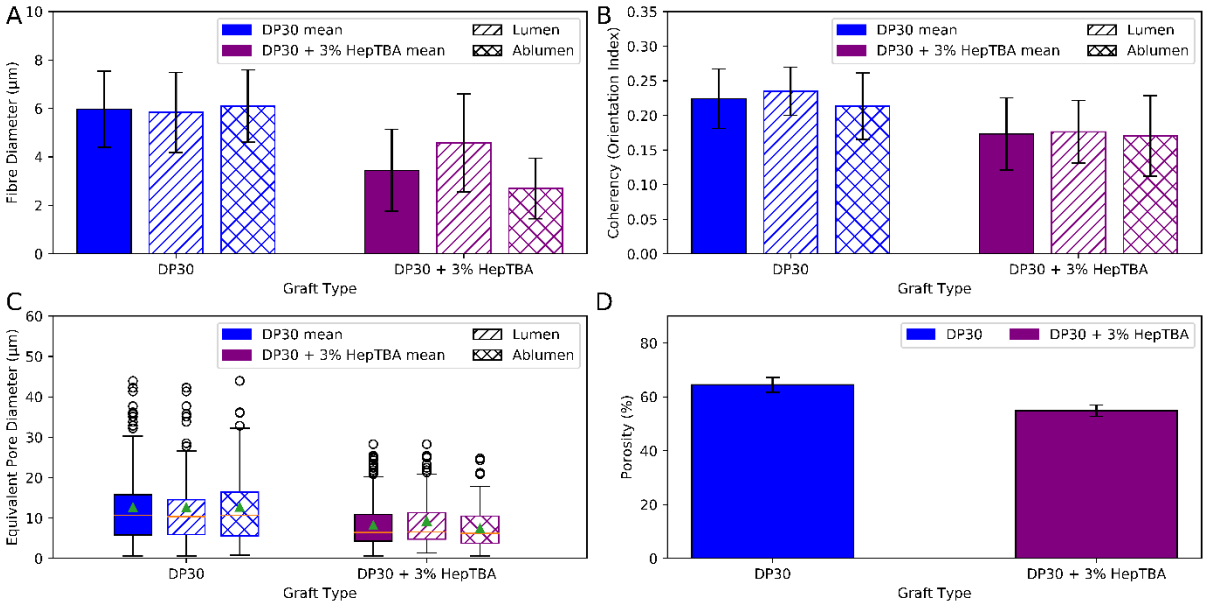

Figure 3-11: *Fibre morphology for DP30 and DP30 + 3% HepTBA electrospun vascular grafts for in vivo pilot study. A) Fibre diameter. B) Fibre coherency (Orientation index). C) Equivalent pore diameter. D) Porosity.*

The same mechanism influences the Taylor cone as this was evident with the decrease of the applied voltage from 11 kV to 7 kV for the pure DP30 and DP30+3%HepTBA, respectively to induce a stable Taylor cone and jet formation.

It should be noted that the applied voltage changed for the 2.1 mm mandrel from the parametric study from 15 kV to 11 kV for the 1.7 mm mandrel, to ensure a stable Taylor cone (50). With this, the mean diameter increased from 4.89±1.31 µm (15 kV) to 5.97±1.57 µm (11 kV) due to a higher degree of stretching of the polymer solution in correlation with the charge repulsion within the polymer jet (130). This is, however, a controversial topic as some research groups found that an increase in voltage increases the fibre diameter due to more solution being ejected from the capillary (131).

Fibre coherency: Both groups were statistically insignificant with a mean OI of 0.199±0.05 which indicates randomly aligned fibres (Figure 3-11 and Table 3-3), that mimics the ECM and will have sufficient mechanical properties in the circumferential and longitudinal direction.

Porosity: The porosity of the grafts was 64.5±2.7% and 54.9±2.2% (P<0.01) for the DP30 and DP30+3%HepTBA, respectively. Table 3-3 illustrates the cross-sectional view of the grafts, showing interconnected pores.

Pore size: The mean pore size of the DP30 and DP30+3%HepTBA were 12.66±9.57 µm (52% of the total pores were larger than 10 µm) and 8.25±5.73 µm (29% of the total pores were larger than 10 µm), respectively. The decrease in pore size ($P<0.0001$) is due to the dependency on fibre diameter, as previously described, larger fibre diameter usually accompanies larger pore sizes. Theoretically, the pore size should also decrease with the production of smaller fibres and a lower porosity (132, 133). The pore size and porosity increased when compared to the 2.1 mm graft (10.9±9.6 µm – pore size, 44.2±7.0% - porosity) and can be attributed to the increase in fibre diameter.

Table 3-3: SEM images of the lumen, ablumen, and cross-sectional area of the DP30 and DP30 + 3% HepTBA electrospun vascular grafts.

Graft type	Lumen	Ablumen	Cross-section
DP30	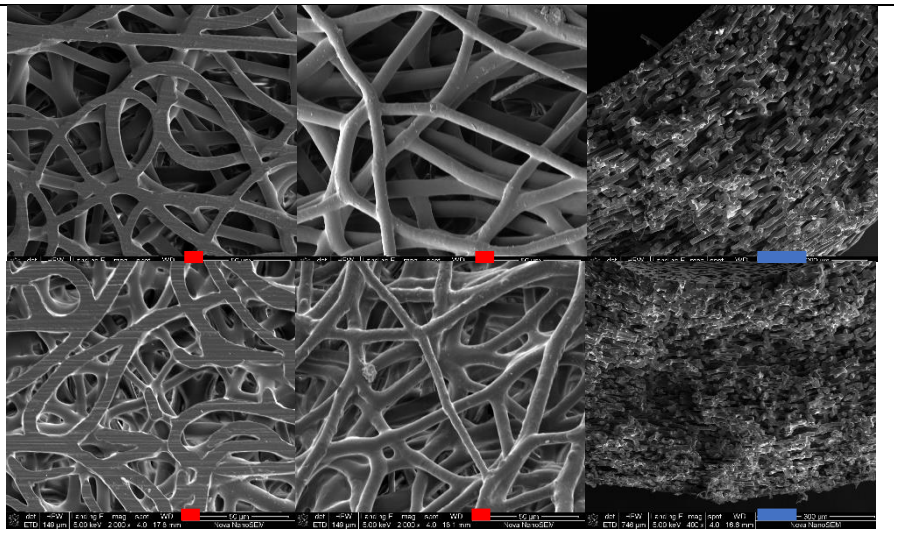		
DP30 + 3% HepTBA			

* Red scale bar = 10 µm. Blue scale bar = 100 µm.

3.3.3 Degradation study

Figure 3-12 shows the change in mechanical properties of the DP30 and DP30 + 3% HepTBA electrospun vascular grafts for a period of 28 days.

UTS: It is clear in Figure 3-12A that the UTS decreases for the DP30 and the DP30 + 3% HepTBA graft from day 0 to 28, in the circumferential and longitudinal direction. The DP30 graft had a circumferential UTS of 0.70±0.16 MPa at day 1 and lost 46% of its tensile strength at day 28 ($P>0.1$), with similar strength loss when compared to day 7 (0.70±0.04 MPa, $P<0.05$). The DP30 + 3% HepTBA had a similar trend, however, it lost 50% of its tensile strength in the circumferential direction, at day 28, compared to day 1 (0.72±0.02 MPa, $P<0.01$). The DP30 and DP30+3% HepTBA had a decrease in longitudinal UTS of 32% from 2.45±0.26 MPa (Day 1, $P<0.05$) and 35% from 2.75±0.09 MPa (Day 1, $P<0.01$) at day 28, respectively.

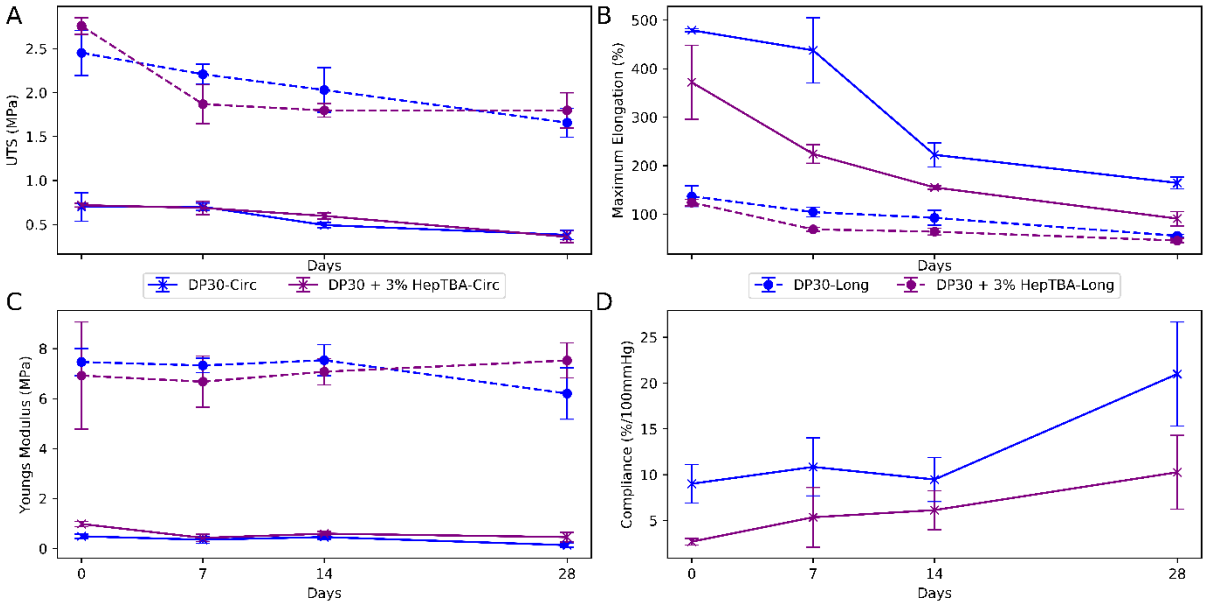

Figure 3-12: *Change in mechanical properties after 0, 7, 14, and 28 days for the DP30 and DP30 + 3% HepTBA electrospun vascular grafts. A) UTS. B) Maximum strain. C) Young's Modulus. D) Compliance.*

Maximum strain: The DP30 and DP30+3% HepTBA had an initial circumferential maximum strain of 479.2±3.5% and 371.9±76.1% with a decrease of 66% ($P<0.0001$) and 76% ($P<0.01$) respectively, at day 28 (Figure 3-12B). The decrease in initial longitudinal strain for DP30 (137.1±21.2%, Day 1) and DP30+3% HepTBA (124.0±6.9%) was 59% ($P<0.01$) and 63% ($P<0.001$), respectively at day 28.

It is evident that the longitudinal UTS is far greater than the UTS in the circumferential direction. This is attributed to the OI of 0.199±0.05, although still random, favouring that of the longitudinal direction. Although the initial circumferential and longitudinal UTS and strains were higher than that compared to Limbert, Omar (114) ($\sigma_{max,\ circ}$ = 1.02±0.23 MPa, $\varepsilon_{max,\ circ}$ = 46±11%, $\sigma_{max,\ long}$ = 0.071±0.016 MPa, $\varepsilon_{max,\ long}$ = 69±24%) the loss in UTS and strain were still similar with 62.7% and 78.3%, respectively. Limbert, Omar (114) had a far greater loss in UTS and strain in the longitudinal direction with 88.7%, and 78.3%, respectively. However, this was due to the fibres that were aligned in the circumferential direction. Interestingly, for both the circumferential and longitudinal UTS, the DP30+3% HepTBA graft had a greater relative decrease in UTS and strain when compared to the DP30 graft. The difference in circumferential and longitudinal UTS was statistically insignificant, although higher values were obtained for the DP30+3%HepTBA due to smaller fibre diameters and less porosity.

Youngs Modulus: Figure 3-12C shows that the degradation study had minimal influence on Young's modulus with no statistical significance between the timepoints for DP30 and DP30+3% HepTBA in the circumferential and longitudinal direction ($P>0.05$). Conversely, a

mean Young's modulus is calculated for the circumferential and longitudinal direction across the time points and groups of 7.09±1.1 MPa and 0.50±0.25 MPa, respectively. The compliance increased for both the groups from day 1 to day 28 as can be seen in Figure 3-12D.

Compliance: Although there was no statistical significance between day 1 to day 28, the DP30 graft increase from 9.0±2.1%/100mmHg to 21.0.3±5.7%/100mmHg with the DP30+3% HepTBA increasing from 2.7±0.4%/100mmHg to 10.3±4.0%/100mmHg.

Grafts should be able to preserve its elastic properties, as many tissues require a certain Young's modulus to thrive and differentiate (134). The consistent Young's modulus for the circumferential as well as the longitudinal direction, allows the graft to keep mechanical integrity and support for cell ingrowth and healing and is in agreement with the findings of Henry, Simonet (135). The elastic properties of polyurethane are dominated by the crystalline segment of the polymer, where the degradation of the urethane occurs. These crystalline arrangements have less accessibility to degradation, therefore any significant changes in Young's modulus were not observed in the time period (136). The compliance of the grafts was in the physiological range even after 28 days of degradation.

3.4 Vascular grafts *in vivo* implantation - Pilot study

The DP30 and DP30+3%HepTBA vascular grafts were implanted to evaluate the healing response *in vivo* in a rat infrarenal aortic implantation model.

3.4.1 Ultrasonography

Figure 3-13 shows the ultrasonographic images of a DP30 implanted graft at day 28. Figure 3-13A and Figure 3-13B shows a longitudinal view of a patent graft at the proximal and distal anastomosis, respectively, confirmed with colour Doppler modalities. Figure 3-13C raised a possible concern that the ultrasonographic images depicted a possible aneurysm, formation of the distal graft. On explant, it was noted that there was no dilatation of the graft evident, with an ID of 1.7 mm. The dilated appearance on imaging could be attributed to the entrapment of air in the small bowel due to adhesions surrounding the distal graft. The blood flow was constant throughout the pilot study with a velocity of approximately 600 m/s at 350±25 bpm. This along with the colour flow, confirmed the patency of the grafts.

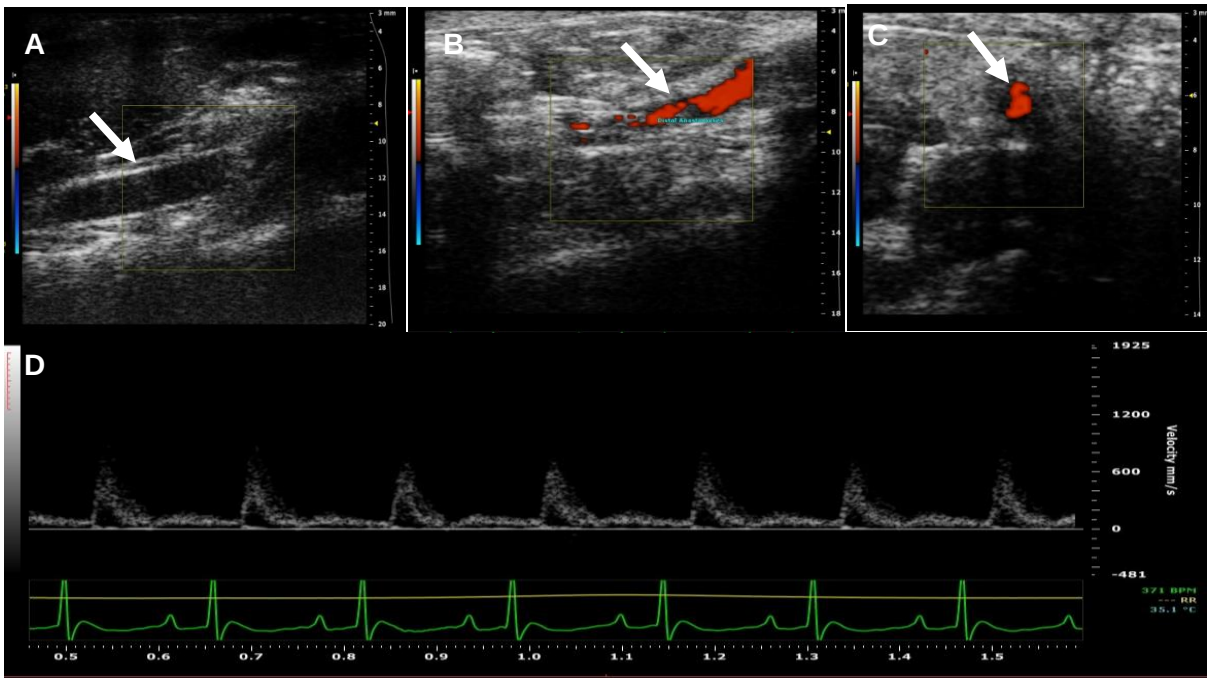

Figure 3-13: *Ultrasonography of DP30 graft at day 28. A) Proximal. B) Distal. C) Cross-sectional. D) Blood velocity.*

Figure 3-14B angiography clearly showing the patency of the graft with contrast visible at the aortic bifurcation into the iliac arteries. All grafts (N = 3, both groups) were patent, therefore unable to distinguish whether the HepTBA inclusion had an influence on the anti-thrombotic lumen.

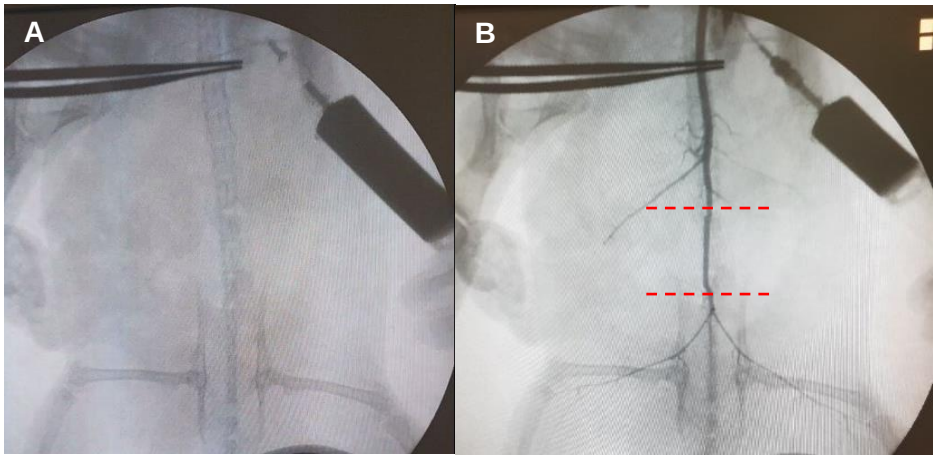

Figure 3-14: *Angiography of graft DP30+3%HepTBA graft at day 28: A) No contrast. B) Contrast injected showing patency of the graft. The red dotted lines indicate the proximal and distal anastomoses.*

Figure 3-15 are images of the DP30 and DP30+3%HepTBA grafts, prior to explantation. It is evident that both Figure 3-15A and Figure 3-15B have bowel with adhesions attached to the graft with vasculature surrounding the graft.

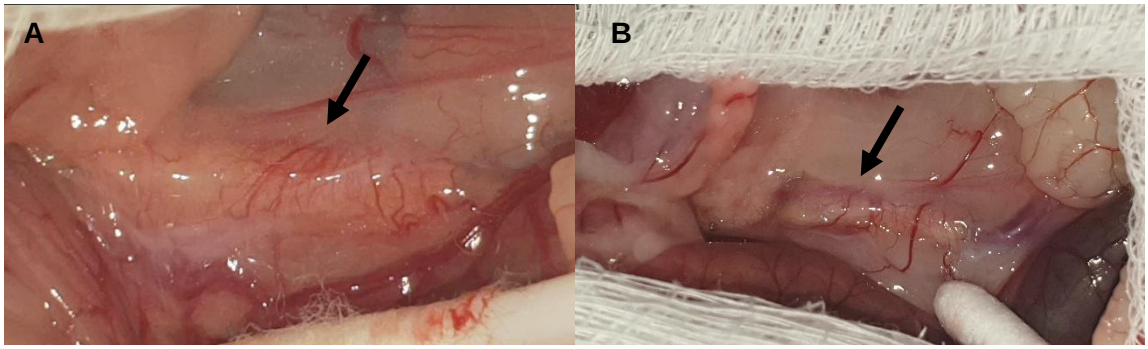

Figure 3-15: *Images of explants showing adhesions. A) DP30. B) DP30+3%HepTBA*

The effects of the inclusion of HepTBA (Figure 3-15B) cannot be confirmed visually with a comparison between the two images (Figure 3-15A and Figure 3-15B) as it seems that there is an equal amount of adhesions to both the grafts as well as vasculature, however this will only be assessed in a long term *in vivo* study.

3.4.2 Histological analysis

An example of endothelialisation is seen in some areas (Figure 3-16), however, this is likely due to TA outgrowth. The differentiation between TA outgrowth and TM vascularisation will be investigated in long term implants using the isolated loop model established in our laboratory (119).

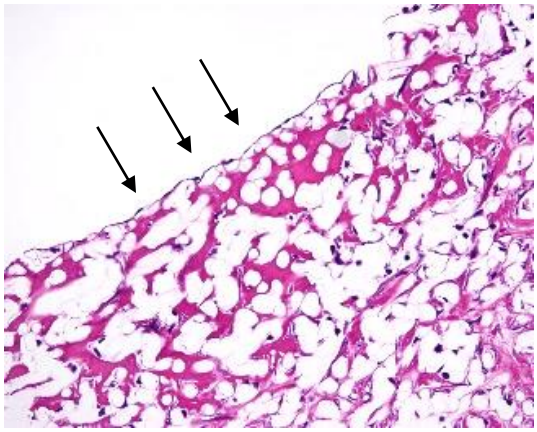

Figure 3-16: *Example of endothelium for the DP30 group.*

Representative micrographs of H&E and Elmas stains of 1 example of the cross-section of a graft for each group are shown in Figure 3-17. Full tissue ingrowth throughout the wall thickness was achieved, apart from some areas near the lumen where fibrin deposits can be seen.

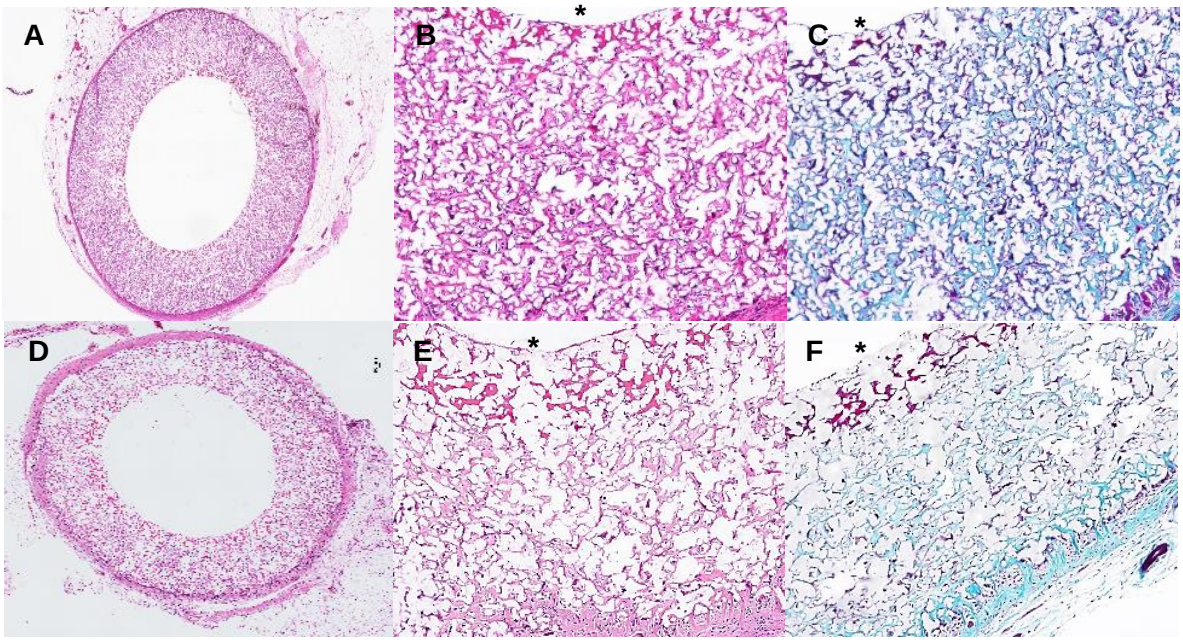

Figure 3-17: *Histological analysis of the DP30 (A-C) and DP30+3%HepTBA (D-F) electrospun vascular grafts used in the pilot study. A, B, D, E) H&E stain of the cross-section (A and D X2 mag, B and E X10 mag). C, F) Miller and Masson elastin trichrome stain for the cross-section (X10). Asterisk (*) denotes the lumen.*

4 Conclusions

This chapter concludes the investigation on the drug incorporation and development of a small diameter biodegradable vascular graft.

- The electrospinning rig with a humidity control unit was successfully designed and upgraded the rH being maintained at the desired set point.
- Neither rH nor the inclusion of HFIP to the solution had a significant effect on the fibre morphology for the rH range and HFIP concentration used as input parameters. In some combinations, the ablumen had an increase in OI and pore size than that of the lumen. Interestingly, the addition of HFIP had an initial increase in porosity but a decrease in average pore size. The addition of HFIP led to a large decrease in UTS and strain in the circumferential direction, whereas the increase in rH had a slight increase in these properties. The longitudinal mechanical properties were not significantly affected by the increase in rH or HFIP concentration.
- HepTBA was successfully incorporated into scaffolds by means of blend electrospinning. The drug release curves were similar for both the concentrations of HepTBA incorporated and had an initial burst release of drug in the first 5 days.
- The inclusion of HepTBA caused a slight decrease in the fibre diameter, OI, pore size and porosity, which was expected with the effects on fibre morphology in electrospinning with the addition of a salt to the polymer solution,
- Similar mechanical properties were however, obtained when HepTBA was incorporated, with a slight decrease in maximum elongation and compliance. Both the scaffolds had a decrease in the UTS and maximum strain in the longitudinal and circumferential direction at day 28. However, a slight increase in compliance was observed.
- The *in vivo* pilot study showed that full ingrowth was achieved for both the groups, however, the cell ingrowth and vascularisation was not quantified as this was out of the scope for the pilot study. The incorporation of HepTBA shows promising results for the anti-thrombotic and angiogenic properties for a long-term *in vivo* study.

5 Recommendations

The following are recommendations for the continuation of this work:

- Investigating more efficient techniques for the removal of the scaffold from the small diameter mandrel.
- Using co-axial electrospinning techniques to incorporate heparin in the core of the DP30 fibre. this may obviate the need for the heparin modification to HepTBA as aqueous solutions may be used for the core.
- Having long-term drug elution studies to determine when remaining HepTBA does elute from with the degradation of the polymer/scaffold.
- Investigating the effects of the HepTBA incorporated scaffolds in a long-term study with the isolated infrarenal loop model (previously established by this research group) to determine its healing response and to distinguish between TA and TM endothelialisation.

6 Research Outputs

Local Conferences Presentation

Vincent Martin Hülk, Anel Oosthuysen, Tim Pennel, Natercia da Silva, Peter Zilla, Deon Bezuidenhout. **Electrospun vascular grafts for tissue engineering.** Del Kahn Surgery Research Day, November 2018

7 References

1. World Health Organisation. South Africa: WHO statistical profile. In: Organization WH, editor. 2015.
2. Roger VL, Go AS, Lloyd-Jones DM, Adams RJ, Berry JD, Brown TM, et al. Heart disease and stroke statistics--2011 update: a report from the American Heart Association. Circulation. 2011;123(4):e18-e209.
3. Stehouwer CD, Clement D, Davidson C, Diehm C, Elte JW, Lambert M, et al. Peripheral arterial disease: a growing problem for the internist. Eur J Intern Med. 2009;20(2):132-8.
4. Stegemann JP, Kaszuba SN, Rowe SL. Review: advances in vascular tissue engineering using protein-based biomaterials. Tissue Eng. 2007;13(11):2601-13.
5. Chlupáč J, Filová E, Bačáková L. Blood Vessel Replacement: 50 years of Development and Tissue Engineering Paradigms in Vascular Surgery. Physiological Research. 2009;58(2):20.
6. Ratcliffe A. Tissue engineering of vascular grafts. Matrix Biol. 2000;19(4):353-7.
7. Hasan A, Memic A, Annabi N, Hossain M, Paul A, Dokmeci MR, et al. Electrospun scaffolds for tissue engineering of vascular grafts. Acta Biomater. 2014;10(1):11-25.
8. Goldman S, Sethi GK, Holman W, Thai H, McFalls E, Ward HB, et al. Radial artery grafts vs saphenous vein grafts in coronary artery bypass surgery: a randomized trial. JAMA. 2011;305(2):167-74.
9. Bouten CV, Dankers PY, Driessen-Mol A, Pedron S, Brizard AM, Baaijens FP. Substrates for cardiovascular tissue engineering. Adv Drug Deliv Rev. 2011;63(4-5):221-41.
10. Wise SG, Byrom MJ, Waterhouse A, Bannon PG, Weiss AS, Ng MK. A multilayered synthetic human elastin/polycaprolactone hybrid vascular graft with tailored mechanical properties. Acta Biomater. 2011;7(1):295-303.
11. Steinhoff G, Stock U, Karim N, Mertsching H, Timke A, Meliss RR, et al. Tissue engineering of pulmonary heart valves on allogenic acellular matrix conduits: in vivo restoration of valve tissue. Circulation. 2000;102(19 Suppl 3):III50-5.
12. McKenna KA, Hinds MT, Sarao RC, Wu PC, Maslen CL, Glanville RW, et al. Mechanical property characterization of electrospun recombinant human tropoelastin for vascular graft biomaterials. Acta Biomater. 2012;8(1):225-33.
13. Kohler TR, Stratton JR, Kirkman TR, Johansen KH, Zierler BK, Clowes AW. Conventional versus high-porosity polytetrafluoroethylene grafts: clinical evaluation. Surgery. 1992;112(5):901-7.
14. Golden MA, Hanson SR, Kirkman TR, Schneider PA, Clowes AW. Healing of polytetrafluoroethylene arterial grafts is influenced by graft porosity. J Vasc Surg. 1990;11(6):838-44; discussion 45.
15. Pennel T, Zilla P, Bezuidenhout D. Biomaterials in Vascular Graft Surgery. Reference Module in Materials Science and Materials Engineering2016.
16. Quarmby JW, Burnand KG, Lockhart SJ, Donald AE, Sommerville KM, Jamieson CW, et al. Prospective randomized trial of woven versus collagen-impregnated knitted prosthetic Dacron grafts in aortoiliac surgery. Br J Surg. 1998;85(6):775-7.
17. Jeschke MG, Hermanutz V, Wolf SE, Koveker GB. Polyurethane vascular prostheses decreases neointimal formation compared with expanded polytetrafluoroethylene. J Vasc Surg. 1999;29(1):168-76.
18. Seifalian AM, Salacinski HJ, Tiwari A, Edwards A, Bowald S, Hamilton G. In vivo biostability of a poly(carbonate-urea)urethane graft. Biomaterials. 2003;24(14):2549-57.
19. Veith FJ, Gupta SK, Ascer E, White-Flores S, Samson RH, Scher LA, et al. Six-year prospective multicenter randomized comparison of autologous saphenous vein and expanded polytetrafluoroethylene grafts in infrainguinal arterial reconstructions. J Vasc Surg. 1986;3(1):104-14.
20. Blumenberg RM, Gelfand ML, Barton EA, Bowers CA, Gittleman DA. Clinical significance of aortic graft dilation. J Vasc Surg. 1991;14(2):175-80.
21. Roll S, Muller-Nordhorn J, Keil T, Scholz H, Eidt D, Greiner W, et al. Dacron vs. PTFE as bypass materials in peripheral vascular surgery--systematic review and meta-analysis. BMC Surg. 2008;8:22.
22. Vacanti JP, Langer R. Tissue engineering: the design and fabrication of living replacement devices for surgical reconstruction and transplantation. The Lancet. 1999;354:S32-S4.
23. Zilla P, Bezuidenhout D, Human P. Prosthetic vascular grafts: wrong models, wrong questions and no healing. Biomaterials. 2007;28(34):5009-27.
24. Wu W, Allen RA, Wang Y. Fast-degrading elastomer enables rapid remodeling of a cell-free synthetic graft into a neoartery. Nat Med. 2012;18(7):1148-53.

25. Wesolowski SA, Fries CC, McMahon JD, Martinez A. Evaluation of a new vascular prosthesis with optimal specifications. Surgery. 1966;59(1):40-56.
26. Hibino N, McGillicuddy E, Matsumura G, Ichihara Y, Naito Y, Breuer C, et al. Late-term results of tissue-engineered vascular grafts in humans. J Thorac Cardiovasc Surg. 2010;139(2):431-6, 6 e1-2.
27. Shin'oka T, Matsumura G, Hibino N, Naito Y, Watanabe M, Konuma T, et al. Midterm clinical result of tissue-engineered vascular autografts seeded with autologous bone marrow cells. J Thorac Cardiovasc Surg. 2005;129(6):1330-8.
28. Matsumura G, Isayama N, Matsuda S, Taki K, Sakamoto Y, Ikada Y, et al. Long-term results of cell-free biodegradable scaffolds for in situ tissue engineering of pulmonary artery in a canine model. Biomaterials. 2013;34(27):6422-8.
29. Yokota T, Ichikawa H, Matsumiya G, Kuratani T, Sakaguchi T, Iwai S, et al. In situ tissue regeneration using a novel tissue-engineered, small-caliber vascular graft without cell seeding. J Thorac Cardiovasc Surg. 2008;136(4):900-7.
30. Lamba N, Woodhouse K, Cooper S. Polyurethanes in Biomedical Applications. Boca Raton: CRC Press.; 1997.
31. Zdrahala R. Small caliber vascular grafts. Part II: Polyurethanes revisited. J Biomater Appl. 1996;11(1):37-61.
32. Saad B, Matter S, Ciardelli G, Uhlschmid GK, Welti M, Neuenschwander P, et al. Interactions of osteoblasts and macrophages with biodegradable and highly porous polyesterurethane foam and its degradation products. J Biomed Mater Res. 1996;32(3):355-66.
33. Krynauw H, Bruchmuller L, Bezuidenhout D, Zilla P, Franz T. Degradation-induced changes of mechanical properties of an electro-spun polyester-urethane scaffold for soft tissue regeneration. J Biomed Mater Res B Appl Biomater. 2011;99(2):359-68.
34. Lane DA, Ryan K. Heparin and low molecular weight heparin: is anti-factor Xa activity important? J Lab Clin Med. 1989;114(4):331-3.
35. Berry D, Shriver Z, Natke B, Kwan CP, Venkataraman G, Sasisekharan R. Heparan sulphate glycosaminoglycans derived from endothelial cells and smooth muscle cells differentially modulate fibroblast growth factor-2 biological activity through fibroblast growth factor receptor-1. Biochem J. 2003;373(Pt 1):241-9.
36. Petitou M, Casu B, Lindahl U. 1976-1983, a critical period in the history of heparin: the discovery of the antithrombin binding site. Biochimie. 2003;85(1-2):83-9.
37. Lee J, Yoo JJ, Atala A, Lee SJ. Controlled heparin conjugation on electrospun poly(epsilon-caprolactone)/gelatin fibers for morphology-dependent protein delivery and enhanced cellular affinity. Acta Biomater. 2012;8(7):2549-58.
38. Chung YI, Kim SK, Lee YK, Park SJ, Cho KO, Yuk SH, et al. Efficient revascularization by VEGF administration via heparin-functionalized nanoparticle-fibrin complex. J Control Release. 2010;143(3):282-9.
39. Lee J, Yoo JJ, Atala A, Lee SJ. The effect of controlled release of PDGF-BB from heparin-conjugated electrospun PCL/gelatin scaffolds on cellular bioactivity and infiltration. Biomaterials. 2012;33(28):6709-20.
40. Lee JY, Choo JE, Choi YS, Lee KY, Min DS, Pi SH, et al. Characterization of the surface immobilized synthetic heparin binding domain derived from human fibroblast growth factor-2 and its effect on osteoblast differentiation. J Biomed Mater Res A. 2007;83(4):970-9.
41. Ceccarelli M, Bani D, Cinci L, Nistri S, Uliva C, Ragazzo E, et al. Anti-inflammatory effects of low molecular weight heparin derivative in a rat model of carrageenan-induced pleurisy. J Cell Mol Med. 2009;13(8B):2704-12.
42. Young E. The anti-inflammatory effects of heparin and related compounds. Thromb Res. 2008;122(6):743-52.
43. McLuckie M, Schmidt CA, Oosthuysen A, Sanchez-Macedo N, Merker H, Bezuidenhout D, et al. High heparin content surface-modified polyurethane discs promote rapid and stable angiogenesis in full thickness skin defects through VEGF immobilization. J Biomed Mater Res A. 2017;105(9):2543-50.
44. Bezuidenhout D, Davies N, Black M, Schmidt C, Oosthuysen A, Zilla P. Covalent surface heparinization potentiates porous polyurethane scaffold vascularization. J Biomater Appl. 2010;24(5):401-18.
45. Sakiyama-Elbert SE. Incorporation of heparin into biomaterials. Acta Biomater. 2014;10(4):1581-7.
46. Barnes CP, Sell SA, Boland ED, Simpson DG, Bowlin GL. Nanofiber technology: designing the next generation of tissue engineering scaffolds. Adv Drug Deliv Rev. 2007;59(14):1413-33.
47. Courtney T, Sacks MS, Stankus J, Guan J, Wagner WR. Design and analysis of tissue engineering scaffolds that mimic soft tissue mechanical anisotropy. Biomaterials. 2006;27(19):3631-8.

48. Zhang Z, Wang Z, Liu S, Kodama M. Pore size, tissue ingrowth, and endothelialization of small-diameter microporous polyurethane vascular prostheses. Biomaterials. 2004;25(1):177-87.
49. Grasl C, Bergmeister H, Stoiber M, Schima H, Weigel G. Electrospun polyurethane vascular grafts: in vitro mechanical behavior and endothelial adhesion molecule expression. J Biomed Mater Res A. 2010;93(2):716-23.
50. Taylor GI. Electrically driven jets. Proceedings of the Royal Society of London A Mathematical and Physical Sciences. 1969;313(1515):453-75.
51. Bhardwaj N, Kundu SC. Electrospinning: a fascinating fiber fabrication technique. Biotechnol Adv. 2010;28(3):325-47.
52. Doshi J, Reneker DH. Electrospinning process and applications of electrospun fibers. Journal of Electrostatics. 1993;35(2-3):160.
53. Deitzel JM, Kleinmeyer J, Harris D, Beck Tan NC. The effect of processing variables on the morphology of electrospun nanofibers and textiles. Polymer. 2001;42(1):272.
54. Eda G, Shivkumar S. Bead-to-fiber transition in electrospun polystyrene. Journal of Applied Polymer Science. 2007;106(1):475-87.
55. Fong H, Chun I, Reneker DH. Beaded nanofibers formed during electrospinning. Polymer. 1999;40(16):4585-92.
56. Yang Q, Li Z, Hong Y, Zhao Y, Qiu S, Wang C, et al. Influence of solvents on the formation of ultrathin uniform poly(vinyl pyrrolidone) nanofibers with electrospinning. Journal of Polymer Science Part B: Polymer Physics. 2004;42(20):3721-6.
57. Li Z, Wang C. Effects of Working Parameters on Electrospinning. One-Dimensional nanostructures. SpringerBriefs in Materials2013. p. 15-28.
58. Demir MM, Yilgor I, Yilgor E, Erman B. Electrospinning of polyurethane fibers. Polymer. 2002;43(11):3303-9.
59. Baumgarten PK. Electrostatic spinning of acrylic microfibers. Journal of Colloid and Interface Science. 1971;36(1):71-9.
60. Zong X, Kim K, Fang D, Ran S, Hsiao BS, Chu B. Structure and process relationship of electrospun bioabsorbable nanofiber membranes. Polymer. 2002;43(16):4403-12.
61. Megelski S, Stephens JS, Chase DB, Rabolt JF. Micro- and Nanostructured Surface Morphology on Electrospun Polymer Fibers. Macromolecules. 2002;35(22):8456-66.
62. Nezarati RM, Eifert MB, Cosgriff-Hernandez E. Effects of humidity and solution viscosity on electrospun fiber morphology. Tissue Eng Part C Methods. 2013;19(10):810-9.
63. De Vrieze S, Van Camp T, Nelvig A, Hagström B, Westbroek P, De Clerck K. The effect of temperature and humidity on electrospinning. Journal of Materials Science. 2009;44(5):1357-62.
64. Sarkar S, Salacinski HJ, Hamilton G, Seifalian AM. The mechanical properties of infrainguinal vascular bypass grafts: their role in influencing patency. Eur J Vasc Endovasc Surg. 2006;31(6):627-36.
65. Ballyk PD, Walsh C, Butany J, Ojha M. Compliance mismatch may promote graft-artery intimal hyperplasia by altering suture-line stresses. J Biomech. 1998;31(3):229-37.
66. Haruguchi H, Teraoka S. Intimal hyperplasia and hemodynamic factors in arterial bypass and arteriovenous grafts: a review. J Artif Organs. 2003;6(4):227-35.
67. Greenwald SE, Berry CL. Improving vascular grafts: the importance of mechanical and haemodynamic properties. J Pathol. 2000;190(3):292-9.
68. Salacinski HJ, Goldner S, Giudiceandrea A, Hamilton G, Seifalian AM, Edwards A, et al. The mechanical behavior of vascular grafts: a review. J Biomater Appl. 2001;15(3):241-78.
69. L'Heureux N, Dusserre N, Marini A, Garrido S, de la Fuente L, McAllister T. Technology insight: the evolution of tissue-engineered vascular grafts--from research to clinical practice. Nat Clin Pract Cardiovasc Med. 2007;4(7):389-95.
70. Stekelenburg M, Rutten MC, Snoeckx LH, Baaijens FP. Dynamic straining combined with fibrin gel cell seeding improves strength of tissue-engineered small-diameter vascular grafts. Tissue Eng Part A. 2009;15(5):1081-9.
71. Stitzel J, Liu J, Lee SJ, Komura M, Berry J, Soker S, et al. Controlled fabrication of a biological vascular substitute. Biomaterials. 2006;27(7):1088-94.
72. Ekaputra AK, Prestwich GD, Cool SM, Hutmacher DW. Combining electrospun scaffolds with electrosprayed hydrogels leads to three-dimensional cellularization of hybrid constructs. Biomacromolecules. 2008;9(8):2097-103.
73. Soletti L, Hong Y, Guan J, Stankus JJ, El-Kurdi MS, Wagner WR, et al. A bilayered elastomeric scaffold for tissue engineering of small diameter vascular grafts. Acta Biomater. 2010;6(1):110-22.
74. Vaz CM, van Tuijl S, Bouten CV, Baaijens FP. Design of scaffolds for blood vessel tissue engineering using a multi-layering electrospinning technique. Acta Biomater. 2005;1(5):575-82.

75. He W, Ma Z, Teo WE, Dong YX, Robless PA, Lim TC, et al. Tubular nanofiber scaffolds for tissue engineered small-diameter vascular grafts. J Biomed Mater Res A. 2009;90(1):205-16.
76. Kwon IK, Matsuda T. Co-electrospun nanofiber fabrics of poly(L-lactide-co-epsilon-caprolactone) with type I collagen or heparin. Biomacromolecules. 2005;6(4):2096-105.
77. Yin A, Luo R, Li J, Mo X, Wang Y, Zhang X. Coaxial electrospinning multicomponent functional controlled-release vascular graft: Optimization of graft properties. Colloids Surf B Biointerfaces. 2017;152:432-9.
78. Clowes AW, Karnowsky MJ. Suppression by heparin of smooth muscle cell proliferation in injured arteries. Nature. 1977;265(5595):625-6.
79. Folkman J, Shing Y. Control of angiogenesis by heparin and other sulfated polysaccharides. Adv Exp Med Biol. 1992;313:355-64.
80. Soletti L, Nieponice A, Hong Y, Ye SH, Stankus JJ, Wagner WR, et al. In vivo performance of a phospholipid-coated bioerodable elastomeric graft for small-diameter vascular applications. J Biomed Mater Res A. 2011;96(2):436-48.
81. Milleret V, Hefti T, Hall H, Vogel V, Eberli D. Influence of the fiber diameter and surface roughness of electrospun vascular grafts on blood activation. Acta Biomater. 2012;8(12):4349-56.
82. Evrova O, Houska J, Welti M, Bonavoglia E, Calcagni M, Giovanoli P, et al. Bioactive, Elastic, and Biodegradable Emulsion Electrospun DegraPol Tube Delivering PDGF-BB for Tendon Rupture Repair. Macromol Biosci. 2016;16(7):1048-63.
83. Meier Burgisser G, Calcagni M, Muller A, Bonavoglia E, Fessel G, Snedeker JG, et al. Prevention of peritendinous adhesions using an electrospun DegraPol polymer tube: a histological, ultrasonographic, and biomechanical study in rabbits. Biomed Res Int. 2014;2014:656240.
84. Hufnagel CA. Permanent intubation of the thoracic aorta. Arch Surg. 1947;54(4):382-9.
85. Voorneveld J, Oosthuysen A, Franz T, Zilla P, Bezuidenhout D. Dual electrospinning with sacrificial fibers for engineered porosity and enhancement of tissue ingrowth. J Biomed Mater Res B Appl Biomater. 2017;105(6):1559-72.
86. Florey HW, Greer SJ, Kiser J, Poole JC, Telander R, Werthessen NT. The development of the pseudointima lining fabric grafts of the aorta. Br J Exp Pathol. 1962;43:655-60.
87. Yong NK, Kinmonth JB, Taylor GW. The Endothelial Lining of Vascular Grafts. Surg Gynecol Obstet. 1963;117:305-10.
88. Berger K, Sauvage LR, Rao AM, Wood SJ. Healing of arterial prostheses in man: its incompleteness. Ann Surg. 1972;175(1):118-27.
89. Pennel T, Zilla P, Bezuidenhout D. Differentiating transmural from transanastomotic prosthetic graft endothelialization through an isolation loop-graft model. J Vasc Surg. 2013;58(4):1053-61.
90. Rocco KA, Maxfield MW, Best CA, Dean EW, Breuer CK. In vivo applications of electrospun tissue-engineered vascular grafts: a review. Tissue Eng Part B Rev. 2014;20(6):628-40.
91. Hashi CK, Zhu Y, Yang GY, Young WL, Hsiao BS, Wang K, et al. Antithrombogenic property of bone marrow mesenchymal stem cells in nanofibrous vascular grafts. Proc Natl Acad Sci U S A. 2007;104(29):11915-20.
92. Pektok E, Nottelet B, Tille JC, Gurny R, Kalangos A, Moeller M, et al. Degradation and healing characteristics of small-diameter poly(epsilon-caprolactone) vascular grafts in the rat systemic arterial circulation. Circulation. 2008;118(24):2563-70.
93. Nottelet B, Pektok E, Mandracchia D, Tille JC, Walpoth B, Gurny R, et al. Factorial design optimization and in vivo feasibility of poly(epsilon-caprolactone)-micro- and nanofiber-based small diameter vascular grafts. J Biomed Mater Res A. 2009;89(4):865-75.
94. Innocente F, Mandracchia D, Pektok E, Nottelet B, Tille JC, de Valence S, et al. Paclitaxel-eluting biodegradable synthetic vascular prostheses: a step towards reduction of neointima formation? Circulation. 2009;120(11 Suppl):S37-45.
95. Tillman BW, Yazdani SK, Lee SJ, Geary RL, Atala A, Yoo JJ. The in vivo stability of electrospun polycaprolactone-collagen scaffolds in vascular reconstruction. Biomaterials. 2009;30(4):583-8.
96. Hong Y, Ye SH, Nieponice A, Soletti L, Vorp DA, Wagner WR. A small diameter, fibrous vascular conduit generated from a poly(ester urethane)urea and phospholipid polymer blend. Biomaterials. 2009;30(13):2457-67.
97. Nieponice A, Soletti L, Guan J, Hong Y, Gharaibeh B, Maul TM, et al. In vivo assessment of a tissue-engineered vascular graft combining a biodegradable elastomeric scaffold and muscle-derived stem cells in a rat model. Tissue Eng Part A. 2010;16(4):1215-23.
98. Hashi CK, Derugin N, Janairo RR, Lee R, Schultz D, Lotz J, et al. Antithrombogenic modification of small-diameter microfibrous vascular grafts. Arterioscler Thromb Vasc Biol. 2010;30(8):1621-7.

99. de Valence S, Tille JC, Mugnai D, Mrowczynski W, Gurny R, Moller M, et al. Long term performance of polycaprolactone vascular grafts in a rat abdominal aorta replacement model. Biomaterials. 2012;33(1):38-47.
100. de Valence S, Tille JC, Giliberto JP, Mrowczynski W, Gurny R, Walpoth BH, et al. Advantages of bilayered vascular grafts for surgical applicability and tissue regeneration. Acta Biomater. 2012;8(11):3914-20.
101. Kuwabara F, Narita Y, Yamawaki-Ogata A, Kanie K, Kato R, Satake M, et al. Novel small-caliber vascular grafts with trimeric Peptide for acceleration of endothelialization. Ann Thorac Surg. 2012;93(1):156-63; discussion 63.
102. Zheng W, Wang Z, Song L, Zhao Q, Zhang J, Li D, et al. Endothelialization and patency of RGD-functionalized vascular grafts in a rabbit carotid artery model. Biomaterials. 2012;33(10):2880-91.
103. Ye L, Wu X, Duan HY, Geng X, Chen B, Gu YQ, et al. The in vitro and in vivo biocompatibility evaluation of heparin-poly(epsilon-caprolactone) conjugate for vascular tissue engineering scaffolds. J Biomed Mater Res A. 2012;100(12):3251-8.
104. Bergmeister H, Grasl C, Walter I, Plasenzotti R, Stoiber M, Schreiber C, et al. Electrospun small-diameter polyurethane vascular grafts: ingrowth and differentiation of vascular-specific host cells. Artif Organs. 2012;36(1):54-61.
105. Zhao J, Qiu H, Chen DL, Zhang WX, Zhang DC, Li M. Development of nanofibrous scaffolds for vascular tissue engineering. Int J Biol Macromol. 2013;56:106-13.
106. Lu G, Cui SJ, Geng X, Ye L, Chen B, Feng ZG, et al. Design and preparation of polyurethane-collagen/heparin-conjugated polycaprolactone double-layer bionic small-diameter vascular graft and its preliminary animal tests. Chin Med J (Engl). 2013;126(7):1310-6.
107. Zhai W, Qiu LJ, Mo XM, Wang S, Xu YF, Peng B, et al. Coaxial electrospinning of P(LLA-CL)/heparin biodegradable polymer nanofibers: potential vascular graft for substitution of femoral artery. J Biomed Mater Res B Appl Biomater. 2013.
108. Wang S, Mo XM, Jiang BJ, Gao CJ, Wang HS, Zhuang YG, et al. Fabrication of small-diameter vascular scaffolds by heparin-bonded P(LLA-CL) composite nanofibers to improve graft patency. Int J Nanomedicine. 2013;8:2131-9.
109. Huang C, Wang S, Qiu L, Ke Q, Zhai W, Mo X. Heparin loading and pre-endothelialization in enhancing the patency rate of electrospun small-diameter vascular grafts in a canine model. ACS Appl Mater Interfaces. 2013;5(6):2220-6.
110. Bergmeister H, Schreiber C, Grasl C, Walter I, Plasenzotti R, Stoiber M, et al. Healing characteristics of electrospun polyurethane grafts with various porosities. Acta Biomater. 2013;9(4):6032-40.
111. Bergmeister H, Seyidova N, Schreiber C, Strobl M, Grasl C, Walter I, et al. Biodegradable, thermoplastic polyurethane grafts for small diameter vascular replacements. Acta Biomater. 2015;11:104-13.
112. Hotaling NA, Bharti K, Kriel H, Simon CG, Jr. DiameterJ: A validated open source nanofiber diameter measurement tool. Biomaterials. 2015;61:327-38.
113. Englund-Johansson U, Netanyah E, Johansson F. Tailor-Made Electrospun Culture Scaffolds Control Human Neural Progenitor Cell Behavior—Studies on Cellular Migration and Phenotypic Differentiation. Journal of Biomaterials and Nanobiotechnology. 2017;08(01):1-21.
114. Limbert G, Omar R, Krynauw H, Bezuidenhout D, Franz T. The anisotropic mechanical behaviour of electro-spun biodegradable polymer scaffolds: Experimental characterisation and constitutive formulation. J Mech Behav Biomed Mater. 2016;53:21-39.
115. Krynauw H, Bruchmüller L, Bezuidenhout D, Zilla P, Franz T. Degradation-induced changes of mechanical properties of an electro-spun polyester-urethane scaffold for soft tissue regeneration. Journal of Biomedical Materials Research B. 2011.
116. Milleret V, Simona B, Neuenschwander P, Hall H. Tuning electrospinning parameters for production of 3D-fiber-fleeces with increased porosity for soft tissue engineering applications. Eur Cell Mater. 2011;21:286-303.
117. Jose AD, Collison D. The normal range and determinants of the intrinsic heart rate in man. Cardiovasc Res. 1970;4(2):160-7.
118. Weissler AM, Harris WS, Schoenfeld CD. Systolic time intervals in heart failure in man. Circulation. 1968;37(2):149-59.
119. Pennel T, Bezuidenhout D, Koehne J, Davies NH, Zilla P. Transmural capillary ingrowth is essential for confluent vascular graft healing. Acta Biomater. 2018;65:237-47.
120. Pennel T, Fercana G, Bezuidenhout D, Simionescu A, Chuang TH, Zilla P, et al. The performance of cross-linked acellular arterial scaffolds as vascular grafts; pre-clinical testing in direct and isolation loop circulatory models. Biomaterials. 2014;35(24):6311-22.

121. Theron SA, Zussman E, Yarin AL. Experimental investigation of the governing parameters in the electrospinning of polymer solutions. Polymer. 2004;45(6):2017-30.
122. Soliman S, Pagliari S, Rinaldi A, Forte G, Fiaccavento R, Pagliari F, et al. Multiscale three-dimensional scaffolds for soft tissue engineering via multimodal electrospinning. Acta Biomater. 2010;6(4):1227-37.
123. Ju YM, Choi JS, Atala A, Yoo JJ, Lee SJ. Bilayered scaffold for engineering cellularized blood vessels. Biomaterials. 2010;31(15):4313-21.
124. Wang Z, Cui Y, Wang J, Yang X, Wu Y, Wang K, et al. The effect of thick fibers and large pores of electrospun poly(epsilon-caprolactone) vascular grafts on macrophage polarization and arterial regeneration. Biomaterials. 2014;35(22):5700-10.
125. Milleret V, Simonet M, Bittermann AG, Neuenschwander P, Hall H. Cyto- and hemocompatibility of a biodegradable 3D-scaffold material designed for medical applications. J Biomed Mater Res B Appl Biomater. 2009;91(1):109-21.
126. Riboldi SA, Sampaolesi M, Neuenschwander P, Cossu G, Mantero S. Electrospun degradable polyesterurethane membranes: potential scaffolds for skeletal muscle tissue engineering. Biomaterials. 2005;26(22):4606-15.
127. Horst M, Milleret V, Noetzli S, Gobet R, Sulser T, Eberli D. Polyesterurethane and acellular matrix based hybrid biomaterial for bladder engineering. J Biomed Mater Res B Appl Biomater. 2017;105(3):658-67.
128. Tai NR, Giudiceandrea A, Salacinski HJ, Seifalian AM, Hamilton G. In vivo femoropopliteal arterial wall compliance in subjects with and without lower limb vascular disease. J Vasc Surg. 1999;30(5):936-45.
129. Luong-Van E, Grondahl L, Chua KN, Leong KW, Nurcombe V, Cool SM. Controlled release of heparin from poly(epsilon-caprolactone) electrospun fibers. Biomaterials. 2006;27(9):2042-50.
130. Sill TJ, von Recum HA. Electrospinning: applications in drug delivery and tissue engineering. Biomaterials. 2008;29(13):1989-2006.
131. Garg K, Bowlin GL. Electrospinning jets and nanofibrous structures. Biomicrofluidics. 2011;5(1):13403.
132. Tomadakis MM, Robertson TJ. Survival and relaxation time, pore size distribution moments, and viscous permeability in random unidirectional fiber structures. J Chem Phys. 2005;122(9):094711.
133. Eichhorn SJ, Sampson WW. Relationships between specific surface area and pore size in electrospun polymer fibre networks. J R Soc Interface. 2010;7(45):641-9.
134. Shoichet MS. Polymer Scaffolds for Biomaterials Applications. Macromolecules. 2010;43(2):581-91.
135. Henry JA, Simonet M, Pandit A, Neuenschwander P. Characterization of a slowly degrading biodegradable polyester-urethane for tissue engineering scaffolds. J Biomed Mater Res A. 2007;82(3):669-79.
136. Umare SS, Chandure AS. Synthesis, characterization and biodegradation studies of poly(ester urethane)s. Chemical Engineering Journal. 2008;142(1):65-77.